NASA CONTRACTOR REPORT

NASA CR-1029

NASA CR-1029

EXPERIMENTAL INVESTIGATION OF CONTAINMENT IN CONSTANT-TEMPERATURE RADIAL-INFLOW VORTEXES

by John S. Kendall

Prepared by

UNITED AIRCRAFT CORPORATION

East Hartford, Conn.

for

NATIONAL AERONAUTICS AND SPACE ADMINISTRATION • WASHINGTON, D. C. • MAY 1968

NASA CR-1029

EXPERIMENTAL INVESTIGATION OF CONTAINMENT IN CONSTANT-TEMPERATURE RADIAL-INFLOW VORTEXES

By John S. Kendall

Issued by Originator as Report No. F-910091-15

Prepared under Contract No. NASw-847 by
UNITED AIRCRAFT CORPORATION
East Hartford, Conn.

for

NATIONAL AERONAUTICS AND SPACE ADMINISTRATION

For sale by the Clearinghouse for Federal Scientific and Technical Information
Springfield, Virginia 22151 – CFSTI price $3.00

Experimental Investigation of Containment in

Constant-Temperature Radial-Inflow Vortexes

TABLE OF CONTENTS

Experimental Investigation of Containment in Constant-Temperature Radial-Inflow Vortexes

SUMMARY

An experimental investigation was conducted to determine the containment characteristics of radial-inflow vortexes for potential application to a vortex-stabilized nuclear light bulb engine. This engine concept is based on the transfer of energy by thermal radiation from gaseous nuclear fuel contained in a vortex through an internally cooled transparent wall to seeded hydrogen propellant. A transparent buffer gas would be injected at the inner surface of the transparent wall to drive the vortex and to isolate the wall from the fuel and fission products.

Tests were conducted using 10-in.-dia by 30-in.-long vortex tubes. Air used to simulate the buffer gas was injected through ports in the peripheral walls of the vortex tubes. Iodine mixed with one of four other gases (helium, nitrogen, sulfur hexafluoride or a heavy fluorocarbon, FC-77) was used to simulate the gaseous nuclear fuel. The simulated fuel was injected at several different locations: at one end wall without swirl through 10 small tubes; at one end wall with swirl through 10 wall jets; or radially inward from the peripheral wall through 12 small tubes at the axial mid-plane of the vortex tube. Flow was removed through 1.0-in.-dia thru-flow ports at the center of one or both end walls. Flow also was removed through 1/8-in.-wide annuli at the outer edges of both end walls (axial bypass) or through ports at the peripheral wall (peripheral bypass). The amount and radial distribution of simulated fuel contained in the vortex were determined using an axial light beam absorption technique.

The effects on containment of changes in the following were investigated: (1) the geometry of the simulated-fuel injection configurations, (2) the number of thru-flow ports used, (3) the radial Reynolds number (a measure of the amount of flow withdrawn through the thru-flow ports) and the corresponding amount of bypass flow, and (4) the molecular weight of the simulated fuel.

RESULTS AND CONCLUSIONS

1. When a helium/iodine mixture was used as simulated fuel, little or no simulated fuel was detected near the peripheral wall. The amount of simulated fuel detected near the wall increased when heavier mixtures were used. This result indicates that the favorable radial gradient of density (density increasing with increasing radius) existing when the helium/iodine mixture was used probably reduced turbulent diffusion of simulated fuel outward toward the peripheral wall. If this hypothesis is correct, the favorable gradients that would exist in the buffer region of a nuclear light bulb engine due to radial temperature gradients should also reduce the diffusion of fuel radially outward through the buffer-gas region.

2. Increasing the radial Reynolds number resulted in decreases in the amount of simulated fuel near the peripheral wall. Also, for a given radial Reynolds number, less simulated fuel was detected near the peripheral wall for configurations employing axial bypass than for configurations employing no bypass. However, it is expected that reductions in the amount of simulated fuel near the peripheral wall could be obtained for no-bypass configurations by using smaller simulated-buffer-gas injection areas than were used in this test program.

3. Changes in the location at which thru flow was removed (a port at the center of either end wall or ports in both end walls) did not significantly affect containment. Thus, it is probable that only one thru-flow port would be required in a nuclear light bulb engine.

4. Injection of simulated fuel at one end wall without swirl through 10 small tubes at a radius of 2.5 in. was the most satisfactory simulated-fuel injection configuration tested. Injection at one end wall with swirl and injection radially inward from the peripheral wall at the axial mid-plane resulted in significant simulated-fuel densities near the peripheral wall.

INTRODUCTION

One of the most interesting propulsion concepts for space travel in the post-1975 time period is the gaseous nuclear rocket engine. In this engine concept, heat is transferred by thermal radiation from a gaseous fissioning fuel to a propellant such as hydrogen. Because of the high temperatures obtainable in the gaseous fuel, such engines can theoretically provide values of specific impulse on the order of 1500 to 3000 sec and thrust-to-weight ratios greater than unity. The primary problems associated with such engines are the containment of the gaseous fuel in a cavity and the transfer of heat from the fuel to the propellant. The containment and heat transfer must be accomplished in a manner such that conventional materials and cooling techniques may be used in the containment vessel and exhaust nozzle.

Research on the characteristics of gaseous nuclear rockets has been carried out at a number of Government laboratories (notably the NASA Lewis Research Center, the Jet Propulsion Laboratory, the Aerospace Corporation, and the AEC Oak Ridge National Laboratory) and at a number of private laboratories. The largest research effort in a Government laboratory is being conducted at the NASA Lewis Research Center; this organization has concentrated on investigations of the coaxial-flow reactor concept. The largest research effort in private industry has been conducted at the United Aircraft Research Laboratories (UARL). At present, the purpose of the major portion of the research at UARL is to investigate the feasibility of the nuclear light bulb engine concept (Fig. 1a). This concept is based on the transfer of energy by thermal radiation from gaseous nuclear fuel contained in a vortex to seeded hydrogen propellant passing external to an internally cooled transparent wall located between the fuel-containment and propellant regions. A transparent buffer gas, such as neon, is injected tangent to the inner surface of the transparent peripheral wall. The primary functions of the buffer gas are to drive the vortex and to prevent nuclear fuel and fission products from coming into contact with the transparent wall. Because the transparent wall provides a physical barrier between the fuel and propellant, the nuclear light bulb offers the possibility of perfect containment of fuel and fission products. The work on this concept at the Research Laboratories has been conducted under NASA contracts monitored by the Space Nuclear Propulsion Office (Contracts NASw-847 and NASw-768) and under Corporate sponsorship.

Fluid mechanics experiments have indicated that a radial-inflow vortex appears especially promising for application to the nuclear light bulb engine. The particular radial-inflow flow pattern of interest for this application is characterized by a laminar radial stagnation surface across which there is no convection (Fig. 1b). At this radius, all of the radial flow passes inward through the end-wall boundary layers. The radial stagnation surface can be located as far from the centerline as 80 to 90 percent of the radius of the

vortex tube. In the central region of the vortex tube (inside of the radial stagnation surface), recirculation cells occur. Near the peripheral wall (outside of the radial stagnation surface) the flow has a substantial axial component of velocity. In the nuclear light bulb engine, the gaseous nuclear fuel would be contained in the central region, and any fuel or fission products that diffused radially outward across the radial stagnation surface would be carried axially toward the end walls, down the end wall boundary layers, and out through a thru-flow port (see Fig. 1a) into a fuel recycle system.

Many of the characteristics of radial-inflow vortexes have been investigated in preceding studies at UARL (Refs. 1 through 14) and elsewhere (Refs. 15 through 19). A program in which flow patterns in radial-inflow water vortexes were investigated was conducted concurrently with the containment investigation reported herein (see Ref. 20). The water-vortex program included investigation of the use of axial bypass (flow removal through annuli at the outer edges of the end walls) and peripheral bypass (flow removal through ports in the peripheral wall) as a means for controlling the location of the radial stagnation surface. It was found that, even with no bypass, the radius of the radial stagnation surface could be substantially increased by using very small peripheral-wall injection areas for the simulated-buffer gas. It was also found that the trends observed in the experiments could be predicted using the theory of Ref. 1; that is, the effects of changes in peripheral-wall injection area, radial and tangential Reynolds number, and amount of bypass on the radial location of the radial stagnation surface were in agreement with the trends predicted using the theory.

The primary objectives of the gas-vortex test program reported herein were to determine the effects of changes in the geometry of the vortex tube and various flow conditions on the amount of simulated fuel contained in the vortex and its radial distribution. In particular, it was desired to determine the effects on containment of changes in the following: (1) the geometry of the simulated-fuel-injection configuration, (2) the number of thru-flow ports, (3) the radial Reynolds number and amount of bypass flow, and (4) the molecular weight of the simulated fuel.

TEST EQUIPMENT

Most of the test equipment employed in the present investigation was used in preceding work under Contract NASw-847 and was described in detail in Ref. 21. The essential features of this equipment and details of new test equipment which was constructed are presented in this section.

High Reynolds Number Test Facility

The high Reynolds number test facility which was employed in the tests of Ref. 21 was modified for use in this investigation. A schematic diagram of the facility is shown in Fig. 2. As shown in the schematic diagram, there are three principal flow systems: the simulated-fuel supply system, the simulated-buffer-gas supply system, and the test section and exhaust system.

The simulated-fuel supply system provides a metered quantity of simulated fuel to the test section at the pressure, temperature, and weight-flow rate required for a particular flow condition. For the tests reported herein, the simulated fuel consisted of a mixture of gaseous iodine and any one of four carrier gases: helium (molecular weight $m_F \approx 5$ for the mixture), nitrogen ($m_F \approx 29$), sulfur hexafluoride ($m_F \approx 146$), and a heavy fluorocarbon vapor, FC-77 (a 3M Company product; $m_F \approx 400$). To prevent condensation of the gases, the simulated fuel was heated to approximately 320 F and the pressure in the vortex tube was maintained at 0.9 to 1.0 atm. When a mixture of iodine and helium, nitrogen, or sulfur hexafluoride was used, these gases were heated in the carrier gas preheater shown in Fig. 2. When a mixture of iodine and FC-77 was used, FC-77 vapor was produced from liquid FC-77 in the specially constructed fluorocarbon boiler included in the diagram (Fig. 2). Gaseous iodine was produced in a similar manner. Valves in the simulated-fuel supply system provide control of the fraction of iodine in the simulated-fuel mixture. Control of the amount of iodine is essential to obtaining maximum accuracy of the light absorptometers which were used to determine the density of iodine in the simulated fuel.

The simulated-buffer-gas supply system provides a metered quantity of air from an atmospheric inlet to the test section at the pressure, temperature, and weight-flow rate required for a particular flow condition. A combination steam and electric heater is used to heat the air to the desired temperature of approximately 300 F.

The test section in which the vortex tubes were mounted consists of a 20-in.-ID by 30-in.-long outer cylindrical shell with end flanges. (Details of the vortex tubes employed in this investigation will be described in a following section.) The simulated-buffer gas flows through the outer cylindrical shell and

directly into the injection plenum, an annular space between the vortex tube and the outer cylindrical shell (Fig. 2). The exhaust system consists of valves and associated piping necessary to connect the test section to vacuum pumps.

Axial Absorptometer

An axial light beam absorption technique was used to determine the amount of simulated fuel contained and the radial distribution of simulated-fuel density and partial pressure within the vortex tube. Figure 3 is a schematic diagram of the axial absorptometer showing the optical system. It consists of a 100-watt zirconium arc lamp light source located at the focal plane of two 6-in.-dia f/8 parabolic mirrors (only one is visible in the top view of Fig. 3), a beam selector and scanner, plane mirrors mounted on each of the vortex-tube end walls, a 15-in.-dia f/1.5 focusing lens, an interference filter (40 Å half-width with peak transmission at 5250 Å), and an RCA 6655A photomultiplier tube. Light from the arc lamp reflects from the parabolic mirrors to form two 6-in.-dia parallel light beams. The light beams strike the beam selector which is a flat plate on the scanner that has two small (approximately 3/16-in.-dia) holes drilled 5 1/2 in. apart. Light passing through this plate is in two narrow collimated light beams. The diameter of each light beam can be adjusted by an iris on the plate, and a sliding shutter is used to alternately block the light of each beam. The narrow light beams pass axially through glass windows in the end walls of the vortex to the focusing lens and the photomultiplier tube.

Using this absorptometer, the amount of light absorbed by the iodine at a given radius of the vortex tube was measured. The amount of light absorbed is proportional to the axially-averaged iodine density and, hence, provides a measurement of the simulated-fuel density. The light beam was continuously traversed along the vertical diameter of the vortex tube to determine the radial distribution of simulated fuel. The amount of simulated fuel stored in the vortex was determined from the radial distribution of simulated-fuel density. Further details of the absorptometer and a discussion of the principle of operation are presented in Ref. 21.

Vortex Tubes

Two vortex tubes were employed in this investigation. These tubes were designated by their respective simulated-buffer-gas-injection geometries, viz., the directed-wall-jet vortex tube and the multiple-fixed-port vortex tube. The directed-wall-jet vortex tube was employed for all except one series of tests reported herein, and has been used in preceding tests reported in Ref. 21.

A photograph of the directed-wall-jet vortex tube partially installed in the test section of the high Reynolds number test facility is shown in Fig. 4a. This vortex tube is a 10-in.-ID by 30-in.-long steel tube which has provision for

installation of up to 900 directed-wall-jet inserts in the peripheral wall. Figures 5a and 6a show details of the directed-wall-jet geometries that were used. The inserts were distributed in 5 axial rows spaced at 72 deg intervals around the periphery of the vortex tube. Two different distributions of directed-wall-jet inserts were used; one had 30 inserts in each row and the second had 15 inserts in each row. All inserts were oriented such that the direction of simulated-buffer-gas injection was circumferential. The injection area per insert was 0.0225 sq in., and hence the total simulated-buffer-gas injection areas were A_j = 3.38 and 1.69 sq in.

The multiple-fixed-port vortex tube was used only in the series of tests in which different simulated-fuel injection geometries were investigated. A photograph of this vortex tube partially installed on the test facility is presented in Fig. 4b. Details of the simulated-buffer-gas-injection geometry are presented in Figs. 5b and 6b. The multiple-fixed-port vortex tube is also a 10-in.-ID by 30-in.-long steel cylinder. This vortex tube has 4284 0.062-in.-dia holes drilled inward at an angle of 19 deg with respect to the local tangent (see Fig. 6b). Twenty-four holes located at each of 119 axial stations along the length of the vortex tube were used for injection. An additional 12 rows were covered by peripheral bypass plenums (see Figs. 4b and 5b) located at 90-deg intervals around the periphery. The bypass plenums provide for removal of a portion of the injected simulated-buffer gas through the peripheral wall. Thus, the simulated-buffer-gas injection area for this vortex tube was A_j = 8.75 sq in.

The two vortex tubes were tested with different simulated-buffer-gas injection areas, bypass configurations, thru-flow removal configurations, and simulated-fuel injection configurations to form different "vortex tube geometries." A summary of the vortex tube geometries tested is presented in Table I. Most of the tests were conducted in the directed-wall-jet vortex tube with end walls that allow thru-flow removal through 1.0-in.-dia ports at the centers of both end walls and axial bypass flow removal through 1/8-in.-wide annuli at the outer edges of both end walls. The simulated-fuel-injection configuration which was employed consisted of ten 0.1-in.-ID by 0.125-in.-long tubes located in a 5-in.-dia ring on the left end wall (see Figs. 7a and 8a). These tubes provided simulated-fuel injection in the axial direction only.

For the tests to investigate different simulated-fuel injection configurations, the multiple-fixed-port vortex tube, which has provision for peripheral bypass (see Fig. 5b), was used. Only the right end wall had provision for thru-flow removal through a 1.0-in.-dia port at its center. Two different simulated-fuel injection end walls (the left end wall) were used; these are shown in Figs. 7 and 8. One configuration (Figs. 7a and 8a) was also used with the directed-wall-jet vortex tube geometry and was described previously. The second configuration (Figs. 7b and 8b) provided injection with swirl through ten directed-wall-jet inserts that injected simulated fuel only in the circumferential direction. For

a third simulated-fuel injection configuration (Figs. 7c and 8c), nothing was injected at the left end wall, but simulated fuel was injected in the radial direction through twelve 0.10-in.-ID by 0.5-in.-long tubes in an injector ring on the peripheral wall at the axial mid-plane of the vortex tube.

TEST AND DATA-REDUCTION PROCEDURES

Test Procedures

The flow condition for a typical containment test was specified by a fixed vortex tube geometry operating with fixed Reynolds numbers and fixed weight-flow rates of the simulated-buffer gas and simulated fuel. Vortex tube geometry was specified by the simulated-buffer-gas-injection configuration, the configuration for bypass and thru-flow removal, and the simulated-fuel-injection configuration. For tests employing the directed-wall-jet vortex tube, the simulated-buffer-gas-injection area was also specified.

For tests described herein, the temperature of the simulated-buffer gas at injection was approximately 300 F and the total pressure was between 0.9 and 1.0 atmospheres. Air was used as the simulated-buffer gas in all the tests; thus, $\rho_B = 0.05$ lb/ft^3 and $\mu_B = 1.6 \times 10^{-5}$ lb/ft-sec. The Reynolds numbers were varied by changing the simulated-buffer-gas weight-flow rates.

The tangential injection Reynolds number is defined as

$$Re_{t,j} = \frac{\rho_B V_{\phi,j} r_1}{\mu_B} = \frac{W_B r_1}{A_j \mu_B} \tag{1}$$

where ρ_B and μ_B are the density and laminar viscosity of the simulated-buffer gas at injection, r_1 is the radius of the vortex tube, W_B is the simulated-buffer-gas weight-flow rate, and $V_{\phi,j}$ is the average simulated-buffer-gas-injection velocity. This Reynolds number is a measure of the angular momentum of the simulated-buffer gas at injection into the vortex tube. In this investigation, simulated-buffer-gas weight-flow rates were varied from approximately 0.013 to 0.60 lb/sec, and tangential injection Reynolds numbers were varied from approximately 30,000 to approximately 300,000.

The flow rate of the mixture of simulated-buffer gas and simulated fuel through the thru-flow ports was expressed in terms of a radial Reynolds number. This Reynolds number is defined as

$$Re_r = \frac{W_{B,TF}}{2\pi \mu_B L} \tag{2}$$

where $W_{B,TF}$ is the total weight-flow rate (assumed to be entirely simulated-buffer gas) through the thru-flow ports and L is the length of the vortex tube. Radial Reynolds numbers in this investigation were varied from 0 to approximately 220.

The containment tests were conducted in the following manner. For a given vortex tube geometry, both the simulated-buffer-gas and simulated-fuel flow rates were set. The light beam of the axial absorptometer was traversed along the vertical diameter of the vortex tube at least twice to verify that the total amount of simulated fuel within the vortex tube was constant (i.e., that a steady-state condition had been reached). The time required for a single traverse of the axial light beam was approximately 20 seconds (many times the average residence time for the simulated fuel within the vortex tube). After the existence of steady-state conditions had been verified, repeated traverses were made to measure the radial distribution of simulated fuel in the vortex tube. The flow rates were then reset for the next flow condition and the process was repeated.

Data-Reduction Procedures

One measure of the containment characteristics of a confined vortex flow is the average simulated-fuel density, $\bar{\rho}_F$ (i.e., a volume averaged simulated-fuel density based on the amount of simulated fuel contained within the vortex tube). This average density is given by

$$\bar{\rho}_F = \frac{\mathcal{M}_F}{V} \tag{3}$$

where $\mathcal{M}_F$ is the amount of simulated fuel contained in the vortex tube and V is the total volume of the vortex tube. The amount of simulated fuel contained was determined by averaging data obtained from radial traverses both above and below the centerline of the vortex tube. For most tests reported herein, the average value of simulated fuel stored differed from the value determined from individual upper and lower traverses by less than ± 15 percent. A detailed description of the technique employed to determine the amount of simulated fuel contained within a vortex tube by this method and sample calculations are presented in Appendix III of Ref. 21.

A second containment parameter, related to the previously discussed average simulated-fuel density, is the average partial pressure of simulated fuel. This parameter was obtained directly from the average simulated-fuel density by employing the ideal gas equation of state. The molecular weight m_F of the simulated-fuel mixture was determined from the following equation for ideal gas mixtures:

$$m_F = \frac{1}{\frac{W_I}{W_F\, m_I} + \frac{W_c}{W_F\, m_c}} \tag{4}$$

Then, the average partial pressure of the simulated fuel is given by

$$\bar{p}_F = \frac{\bar{\rho}_F \mathcal{R} T_1}{m_F} \tag{5}$$

A third containment parameter, closely related to the average simulated-fuel partial pressure, is the ratio of $\bar{p}_F$ to the total pressure, P_1, in the vortex tube. This ratio is important because it is directly related to the pressure at which a nuclear light bulb engine must operate (i.e., for a given fuel density required for the critical mass, the total pressure necessary in the engine is determined by the ratio of the average fuel partial pressure to the total pressure in the vortex tube). It was assumed that the radial variation of total pressure within the vortex tube was small compared with the absolute total pressure in the vortex tube and hence, a single value of total pressure was used in determining the ratio of the average simulated-fuel partial pressure to the total pressure at all radii.

Some test results are discussed in terms of the secondary flow parameter, β_t. This parameter was originally developed from theoretical considerations in Ref. 1 and was investigated in some detail in the water-vortex investigation reported in Ref. 20. It has been found useful as an indication of the flow patterns which are likely to exist in vortex tubes for given Reynolds numbers and length-to-diameter ratios. From Ref. 1, the expression for β_t is given by

$$\beta_t = \frac{D}{L} \frac{Re_{t,p}}{Re_r}^{0.8} \tag{6}$$

where $Re_{t,p}$ is an empirically determined tangential Reynolds number for the vortex flow. It is related to the tangential injection Reynolds number, $Re_{t,j}$, of the simulated-buffer gas by

$$Re_{t,p} = Re_{t,j} \frac{V_{\phi,p}}{V_{\phi,j}} \tag{7}$$

where $V_{\phi,p}$ is the average tangential velocity at the vortex tube peripheral wall determined by extrapolating velocity distribution measurements to the wall (see discussion in Ref. 20). The average simulated-buffer-gas-injection velocity $V_{\phi,j}$ is determined from

$$V_{\phi,j} = \frac{W_B}{\rho_B A_j} \tag{8}$$

Values of the secondary flow parameter have been determined for most tests reported herein and are shown on the figures where the data are presented. These

values of β_t were determined in the following manner. Figure 9 in Ref. 20 gives a variation of velocity ratio $V_{\phi,p}/V_{\phi,j}$ with peripheral-wall injection area for a range of tangential injection Reynolds number and vortex tube geometries similar to those for the gas-vortex tests reported herein. From this figure, velocity ratios were determined for each of the vortex tube geometries employed in this study. Having determined the velocity ratio, the value of β_t was calculated using Eq. (6) (Re_r and $Re_{t,j}$ were known from the test conditions and $Re_{t,p}$ was determined from Eq. (7)). The test conditions in Ref. 20 were significantly different from those employed in this investigation (in Ref. 20, a water vortex was used and the data were obtained using a configuration which did not have injection of simulated fuel). However, it is believed that β_t provides an indication of the flow patterns which existed during tests conducted in this investigation. The approximate location of the radial stagnation surface as a function of the secondary flow parameter is presented in Fig. 17 of Ref. 20 for several peripheral-wall injection areas. This figure was used where appropriate as an aid in interpreting the measured simulated-fuel density distributions in the present study. A radial stagnation surface occurs when the weight-flow rate in the end-wall boundary layer is equal to the weight-flow rate of the thru-flow. It is implied that at this radius the net radial velocity in the primary flow is zero, and that radial convection of simulated fuel does not occur across the stagnation surface.

DISCUSSION OF RESULTS

The results are presented in five sections. In the first two sections (Figs. 9 through 12), the results of preliminary tests that resulted in selection of a simulated-fuel-injection configuration and a thru-flow configuration for following tests are presented. In the last three sections (Figs. 13 through 23), results are presented which indicate the effect on containment of changes in the radial Reynolds number, tangential injection Reynolds number at a constant radial Reynolds number, and the molecular weight of the simulated fuel.

Tests with Different Simulated-Fuel-Injection Configurations

These tests were conducted using the multiple-fixed-port vortex tube with peripheral bypass and thru-flow withdrawal at the right end wall only (see Table I and Figs. 4b, 5b, and 6b). Three simulated-fuel-injection configurations were tested: injection from the left end wall without swirl, injection from the left end wall with swirl, and injection from the peripheral wall at the axial mid-plane (see Figs. 7a, b, and c, respectively). A fluorocarbon/iodine mixture was used as simulated fuel; the molecular weight of the mixture was approximately 400.

The results shown in Fig. 9 indicate that end-wall injection without swirl was slightly better than end-wall injection with swirl (compare the open and solid circle symbols). For a given radial Reynolds number (Re_r), higher values of average simulated-fuel density ($\bar{\rho}_F$) and average simulated-fuel partial pressure ($\bar{p}_F$) were obtained without swirl injection than with swirl injection. The shapes of the three curves for the two different end-wall injection configurations are similar. Increases in radial Reynolds number result in decreased containment. The shape of the curve for injection of simulated fuel at the peripheral wall is different from the curves for the end-wall injection configurations. Initial increases in radial Reynolds number resulted in increased amounts of simulated fuel contained up to $Re_r = 100$; further increases in Re_r resulted in decreased containment. This variation with radial Reynolds number of the amount of simulated fuel contained also provides an indication of the primary simulated-fuel loss mechanism. At low Re_r, a large fraction of the simulated fuel stays out near the peripheral wall and is lost through the peripheral bypass ports. As Re_r increases, more simulated fuel moves radially inward away from the peripheral wall, and therefore losses through the peripheral bypass ports decrease. As Re_r is increased above 100, an increasing amount of simulated fuel is drawn into the core on the centerline of the vortex and is then lost through the thru-flow port.

Typical radial distributions of simulated-fuel density and partial pressure from the tests of Fig. 9 are shown in Fig. 10. Data were not obtained at radius ratios less than $r/r_1 = 0.10$ due to blockage of the axial light beam by the

thru-flow port and ducting. The data presented are for a radial Reynolds number of about 100 which corresponds to the optimum value for the configuration with simulated-fuel injection at the peripheral wall (see Fig. 9). These distributions verify that the manner in which the simulated fuel distributes itself in the vortex depends strongly upon the simulated-fuel-injection configuration.

In Fig. 10, the distribution for end-wall injection without swirl (open circles) indicates more simulated fuel near the center of the vortex tube than does the distribution for end-wall injection with swirl (solid circles). Thus, injection of the simulated fuel in the axial direction as in the no-swirl configuration appears to be necessary to cause a high concentration of simulated fuel in the central region of the vortex tube. For some cases, injection of the simulated fuel with swirl resulted in periodic pressure fluctuations in the thru-flow ducts. It is believed that these pressure fluctuations were due to a flow instability similar to that described in Ref. 9. In the tests of Ref. 9 it was observed that under some conditions the annulus of simulated fuel began to rotate eccentrically about the centerline of the vortex tube. The amplitude of this motion increased with increasing simulated-fuel weight-flow rate until the annulus deteriorated and the amount of simulated fuel contained decreased sharply. Reasons for the occurrence of this instability are not completely understood. In the present program, pressure fluctuations were only observed for simulated-fuel injection from the end wall with swirl. In the tests of Ref. 9 the instability and pressure fluctuations occurred when the simulated fuel was injected through a single tube passing through the peripheral wall at the axial mid-plane.

On the basis of these results, it was decided to employ simulated-fuel injection from the left end wall without swirl in all following tests.

Tests with Different Thru-Flow Configurations

This series of tests was conducted using the directed-wall-jet vortex tube with axial bypass and with simulated-fuel injection from the left end wall without swirl (see Table I and Figs. 4a, 5a, 6a, 7a, and 8a). During these tests, thru flow was withdrawn at the left end wall only, at the right end wall only, and at both end walls simultaneously. The total simulated-buffer gas injection area was $A_j = 3.38$ sq in. and the radial Reynolds number was about 100. A sulfur-hexafluoride/iodine mixture (molecular weight of about 146) was used as the simulated fuel.

The results are shown in Figs. 11 and 12. The data indicate that changes in the number of thru-flow ports employed had very little effect on the average simulated-fuel densities and partial pressures that were obtained (Fig. 11). Moreover, the typical radial density distributions in Fig. 12 indicate that the number of thru-flow ports employed does not have a significant effect on the

radial distribution of simulated fuel either. On the basis of these results, it was concluded that the number of thru-flow ports employed was not significant and, hence, all following tests were conducted with thru-flow removal at both end walls.

Tests with Different Radial Reynolds Numbers

In these tests and all following tests, the directed-wall-jet vortex tube was used (see Table I and Figs. 4a, 5a, 6a, 7a, and 8a). The simulated fuel was a sulfur-hexafluoride/iodine mixture having a molecular weight about 146.

The effects of changes in radial Reynolds number on containment are shown in Fig. 13. Increases in $\bar{\rho}_F$ with increases in W_F (i.e., with decreases in W_B/W_F, since W_B was held constant for these tests) were obtained for all radial Reynolds numbers. The results indicate that, at all values of W_B/W_F, the tests at a radial Reynolds number of approximately 106 yielded the highest values of average simulated-fuel density. Thus, there is a trend of increasing $\bar{\rho}_F$ with initial increases in Re_r up to $Re_r \approx 106$, then decreasing $\bar{\rho}_F$ with further increases in Re_r. Trends similar to this were observed previously for configurations having peripheral bypass, instead of axial bypass, and simulated-fuel injection from the peripheral wall, instead of from the end wall without swirl (see the curve with the square symbols in Fig. 9; see also Ref. 9 and Appendix I of Ref. 21). No such trends have been observed for configurations having peripheral bypass and simulated-fuel injection from the end walls with and without swirl (see the other three curves in Fig. 9). Thus, it does not appear possible to identify the factors leading to the trend shown in Fig. 13 from the data taken to date.

Four distributions of simulated-fuel density within the vortex tube are shown in Fig. 14. The distributions presented correspond to those data points in Fig. 13 for which W_B/W_F was approximately 31. As the radial Reynolds number was increased, the amount of simulated fuel near the peripheral wall was decreased due to the increased radial inflow, and the amount in the central region was increased.

Corresponding values of the secondary flow parameter for these flow conditions are shown in the table in Fig. 14. As discussed in the section entitled "TEST AND DATA-REDUCTION PROCEDURES," it is possible to estimate the radius of the radial stagnation surface from estimates of β_t. These estimates indicate that this radius ratio would vary from $r_s/r_1 = 0.5$ at $Re_r = 209$ ($\beta_t = 28$) to $r_s/r_1 = 0.7$ at $Re_r = 106$ ($\beta_t = 55$). The distributions in Fig. 14 for $Re_r = 209$ and 106 indicate that the density of the simulated fuel decreased rapidly with increasing radius approximately up to radius ratios equal to those estimated for the location of the radial stagnation surface. Also note in Fig. 14 that the distributions for $Re_r = 54$ ($\beta_t = 109$) and $Re_r = 0$ ($\beta_t = \infty$) are relatively flat, indicating the possible absence of a well-defined radial stagnation surface. These results at high values of β_t are also in qualitative agreement with the results of Ref. 20. In Ref. 20, for a vortex tube configuration with axial bypass, laminar radial

stagnation surfaces were not observed for values of β_t greater than about 65. As β_t was increased above this value, the stagnation surfaces deteriorated and were no longer discernable.

Tests with Different Tangential Injection Reynolds Numbers

In the preceding tests, the radial Reynolds number was changed while the simulated-buffer-gas weight flow rate (and therefore the tangential injection Reynolds number) was held approximately constant. For comparison with the results of the preceding tests, a few tests were conducted in which no bypass flow was removed, but the tangential injection Reynolds number was varied. The directed-wall-jet vortex tube with a simulated-buffer-gas injection area of A_j = 1.69 sq in. was used. The simulated fuel was a nitrogen/iodine mixture having a molecular weight of approximately 29.

Containment data for three simulated-buffer-gas weight-flow rates which provided three tangential injection Reynolds numbers and radial Reynolds numbers are presented in Fig. 15. Since no bypass flow was used, the tangential injection Reynolds number and radial Reynolds number could not be independently changed. To obtain the data for Fig. 15, Re_r was varied from 56 to 214; β_t was very low and only varied from 14.9 to 11.2 (it can be shown that for a fixed vortex tube geometry, $\beta_t \sim Re_r^{-0.2}$). The data in Fig. 15 do not show any significant effect of $Re_{\phi,j}$ on containment, primarily because the values of β_t are so low. It is shown in Refs. 1 and 20 that these low values of β_t correspond to vortex flow patterns for which no radial stagnation surface would occur; instead, a strong radial inflow is produced in the vortex tube. Corresponding tests at higher values of β_t and no thru-flow could not be performed with the existing vortex test equipment because the injection area was too large.

Radial distributions of simulated-fuel density for the three simulated-buffer-gas weight flow rates of Fig. 15 are shown in Fig. 16. These distributions are all at the same simulated-fuel weight flow rate. The value of β_t is approximately constant for these three distributions and, according to theory, the flow patterns within the vortex tube with no secondary injection should be similar. However, Fig. 16 indicates that substantial differences existed in the density distributions. At the lowest simulated-buffer-gas weight-flow rate (W_B = 0.0132 lb/sec), the simulated-fuel density near the peripheral wall was relatively high. As W_B increased, the density of the simulated fuel near the wall decreased. This implies that different flow patterns were produced as W_B was increased. However, since the changes in W_B cause such small changes in β_t, they alone would not be expected to cause changes in the flow patterns. It is apparent that an interaction with the simulated fuel that is injected into the vortex must cause the changes. This is evidence that even though β_t appears to predict some trends observed in the data, account must also be taken of the disturbance due to the simulated-fuel injection.

It is important to note that the presence of simulated fuel near the peripheral wall in these tests does not mean that a satisfactory no-bypass configuration cannot be obtained. It was shown in Refs. 1 and 20 that values of β_t greater than 20 or 25 are required to establish a flow pattern having a radial stagnation surface. Therefore, by decreasing the peripheral-wall injection area to values less than those used in the present program, β_t could be increased and radial stagnation surfaces should be established with no bypass. This should result in reductions in the amount of simulated fuel near the peripheral wall. However, since it has been found that these two-component flows are influenced by W_B/W_F, it is difficult to estimate just how much the injection area should be decreased.

Radial distributions of simulated-fuel density are shown in Fig. 17 for two test conditions for which the radial Reynolds number and the simulated-fuel weight-flow rate were not changed, while the tangential injection Reynolds number was changed from 59,100 to 268,000 and the corresponding amount of axial bypass was changed from 0 percent to 79 percent. The values of β_t for these two tests were 12.8 for the configuration without bypass and 43.1 for the configuration with bypass. These distributions show that the simulated-fuel density near the peripheral wall was lower with a β_t of 43.1 than with a β_t of 12.8. However, as previously discussed, it is expected that decreases in the simulated-buffer-gas injection area in the no-bypass configuration would result in a distribution of simulated fuel which would be more like that shown in Fig. 17 for the higher value of β_t.

Tests to Determine Effects of Changes in Molecular Weight of Simulated Fuel

To determine the effects of changes in the molecular weight of the simulated fuel on containment and, in particular, on the radial distribution of simulated-fuel density, tests were conducted using the following simulated fuels: (1) helium/iodine mixture, $m_F \approx 5$; (2) nitrogen/iodine mixture, $m_F \approx 29$, and (3) sulfur-hexafluoride/iodine mixture, $m_F \approx 146$. The directed-wall-jet vortex tube was used with two simulated-buffer-gas injection areas (A_j = 1.69 and 3.38 sq in.). All tests were conducted at a radial Reynolds number of approximately Re_r = 110.

The results of these tests are presented in Figs. 18 through 23. The containment data (Figs. 18, 20 and 22) all show the same trend observed in preceding tests; $\bar{\rho}_F$ and $\bar{p}_F$ decreasing with increasing W_B/W_F. The containment data in Fig. 18 for the helium/iodine mixture indicate that values of average partial pressure ratios between approximately 0.04 and 0.16 were obtained. This is a significant result because these average simulated-fuel partial pressure ratios are only slightly less than the values required for the specific nuclear light bulb engine described in Ref. 22 ($\bar{p}_F/P_1$ = 0.21, when $\bar{p}_F$ is based on entire vortex tube volume).

The simulated-fuel density distributions in Fig. 19 for the helium/iodine

mixture indicate that most of the simulated fuel was contained inside a radius ratio of approximately 0.6, and that no simulated fuel was detected outside a radius ratio of 0.8. This result is also significant because it indicates that when there is a strong favorable radial gradient of density (density increasing with increasing radius), there is little diffusion radially outward near the peripheral wall. In the nuclear light bulb engine, strong radial density gradients would occur in the buffer-gas region due to temperature gradients. These density gradients would be relied upon to prevent turbulent diffusion of fuel outward toward the transparent wall.

Comparison of Figs. 19, 21, and 23 indicates that as the molecular weight of the simulated fuel increased from 5 to 146, the radius of the central region of high simulated-fuel density decreased from approximately 0.6 to 0.4 times the outer radius of the vortex tube. Also, as the molecular weight of simulated fuel increased, the average density of simulated fuel which was detected near the vortex tube peripheral wall increased.

REFERENCES

1. Anderson, O.: Theoretical Solutions for the Secondary Flow on the End Wall of a Vortex Tube. United Aircraft Research Laboratories Report R-2494-1, prepared under Contract AF 04(611)-7448, November 1961.

2. Owen, F. S., R. W. Hale, B. V. Johnson, and A. Travers: Experimental Investigation of Characteristics of Confined Jet-Driven Vortex Flows. United Aircraft Research Laboratories Report R-2494-2, prepared under Contract AF 04(611)-7448, November 1961.

3. Anderson, O. L.: Theoretical Effect of Mach Number and Temperature Gradient on Primary and Secondary Flow in a Jet-Driven Vortex. Air Force Systems Command Report RTD-TDR-63-1098, prepared by United Aircraft Research Laboratories, November 1963.

4. Mensing, A. E., and J. S. Kendall: Experimental Investigation of Containment of Gaseous Iodine in a Jet-Driven Vortex. Air Force Systems Command Report RTD-TDR-63-1093, prepared by United Aircraft Research Laboratories, November 1963.

5. Johnson, B. V., A. Travers, and R. W. Hale: Measurements of Flow Patterns in a Jet-Driven Vortex. Air Force Systems Command Report RTD-TDR-63-1094, prepared by United Aircraft Research Laboratories, November 1963.

6. Travers, A., and B. V. Johnson: Measurements of Flow Characteristics in a Basic Vortex Tube. United Aircraft Research Laboratories Report C-910091-2, prepared under Contract NASw-847, September 1964. Also issued as NASA CR-278.

7. Travers, A., and B. V. Johnson: Measurements of Flow Characteristics in an Axial-Flow Vortex Tube. United Aircraft Research Laboratories Report C-910091-3, prepared under Contract NASw-847, September 1964. Also issued as NASA CR-277.

8. Johnson, B. V.: Analysis of Secondary-Flow-Control Methods for Confined Vortex Flows. United Aircraft Research Laboratories Report C-910091-1, prepared under Contract NASw-847, September 1964. Also issued as NASA CR-276.

9. Mensing, A. E., and J. S. Kendall: Experimental Investigation of Containment of a Heavy Gas in a Jet-Driven Light-Gas Vortex. United Aircraft Research Laboratories Report D-910091-4, prepared under Contract NASw-847, March 1965. Also issued as NASA CR-68931.

10. Travers, A.: Experimental Investigation of Peripheral Wall Injection Techniques in a Water Vortex Tube. United Aircraft Research Laboratories Report D-910091-7, prepared under Contract NASw-847, September 1965. Also issued as NASA CR-68867.

11. McFarlin, D. J.: Experimental Investigation of the Effect of Peripheral-Wall Injection Technique on Turbulence in an Air Vortex Tube. United Aircraft Research Laboratories Report D-910091-5, prepared under Contract NASw-847, September 1965. Also issued as NASA CR-68867.

12. Johnson, B. V., and A. Travers: Analytical and Experimental Investigation of Flow Control in a Vortex Tube by End-Wall Suction and Injection. United Aircraft Research Laboratories Report D-910091-8, prepared under Contract NASw-847, September 1965. Also issued as NASA CR-68927.

13. Mensing, A. E., and J. S. Kendall: Experimental Investigation of the Effect of Heavy-to-Light-Gas Density Ratio on Two-Component Vortex Tube Containment Characteristics. United Aircraft Research Laboratories Report D-910091-9, prepared under Contract NASw-847, September 1965. Also issued as NASA CR-68926.

14. Clark, J. W., B. V. Johnson, J. S. Kendall, A. E. Mensing, and A. Travers: Summary of Gaseous Nuclear Rocket Fluid Mechanics Research Conducted Under Contract NASw-847. United Aircraft Research Laboratories Report F-910091-13, May 1967. Also AIAA Preprint No. 67-500, presented at AIAA Third Propulsion Joint Specialist Conference, Washington, D. C., July 17-21, 1967.

15. Rosenzweig, M. L., W. S. Lewellen, and D. H. Ross: Confined Vortex Flows with Boundary Layer Interaction. Aerospace Corporation Report No. ATN-64(9227)-2, February 20, 1964. Also AIAA Journal, Vol. 3, No. 12, December 1964, pp. 2127-2134.

16. Pivrotto, T. J.: Mass-Retention Measurements in a Binary Compressible Vortex Flow. Jet Propulsion Laboratory Technical Report No. 32-864, June 15, 1966.

17. Lewellen, W. S., M. L. Rosenzweig, and D. H. Ross: Effects of Secondary Flows of the Containment of a Heavy Gas in a Vortex. Aerospace Corporation Report No. TDR-469(9210-01)-3, 1965. Also AIAA Preprint No. 65-582, presented at AIAA Propulsion Joint Specialist Conference, Colorado Springs, Colorado, June 14-18, 1965.

18. Chang, C. C., S. W. Chi, and C. M. Chen: Gas-Core Nuclear Rocket Fluid Mechanics Experiments at Catholic University of America. AIAA Preprint No. 67-502, presented at AIAA Third Propulsion Joint Specialist Conference, Washington, D. C., July 17-21, 1967.

19. Roschke, E. J.: Flow Visualization Studies of a Confined, Jet-Driven Water Vortex. Jet Propulsion Laboratory Technical Report 32-1004, September 16, 1966.

20. Travers, A.: Experimental Investigation of Radial-Inflow Vortexes in Jet-Injection and Rotating-Peripheral-Wall Water Vortex Tubes. United Aircraft Research Laboratories Report F-910091-14, prepared under Contract NASw-847, September 1967. To be issued as NASA CR report.

21. Kendall, J. S., A. E. Mensing, and B. V. Johnson: Containment Experiments in Vortex Tubes with Radial Outflow and Large Superimposed Axial Flows. United Aircraft Research Laboratories Report F-910091-12, prepared under Contract NASw-847, May 1967. To be issued as NASA CR report.

22. McLafferty, G. H., and H. E. Bauer: Studies of Specific Nuclear Light Bulb and Open-Cycle Vortex-Stabilized Gaseous Nuclear Rocket Engines. United Aircraft Research Laboratories Report F-910093-37, prepared under Contract NASw-847, September 1967. To be issued as NASA CR report.

LIST OF SYMBOLS

A_j	Simulated-buffer-gas injection area, sq in. or sq ft
$A_{F,j}$	Simulated-fuel injection area, sq in. or sq ft
D	Diameter of vortex tube, ft or in.
L	Length of vortex tube, ft or in.
m_c	Molecular weight of carrier gas in simulated-fuel mixture (Eq. (4))
m_F	Molecular weight of simulated fuel
m_I	Molecular weight of iodine, 254 (Eq. (4))
P_1	Total pressure at vortex tube periphery, lb/ft^2
p_F	Local simulated-fuel partial pressure, lb/ft^2
$\bar{p}_F$	Average simulated-fuel partial pressure, $\frac{\bar{\rho}_F \mathcal{R} T_1}{m_F}$, lb/ft^2
$\mathcal{R}$	Universal gas constant, 1545 ft lb/mole-deg R
Re_r	Radial Reynolds number, $\frac{W_{B,TF}}{2\pi\mu_B L}$, dimensionless
$Re_{t,j}$	Tangential injection Reynolds number based on average injection velocity, $\rho_B V_{\phi,j} r_1/\mu_B$, dimensionless
$Re_{t,p}$	Tangential Reynolds number based on velocity at peripheral wall, $\rho_B V_{\phi,p} r_1/\mu_B$, dimensionless
r	Local radius from centerline of vortex tube, ft or in.
r_s	Radius of radial stagnation surface (see Fig. 1 and Ref. 20), ft or in.
r_1	Radius of vortex tube, ft or in.
T_1	Temperature of simulated-buffer-gas at injection, deg R
V	Volume of vortex tube, $\pi r_1^2 L$, ft^3
$V_{\phi,j}$	Average simulated-buffer-gas injection velocity into vortex tube, $W_B/\rho_B A_j$, ft/sec

$V_{\phi,p}$ Tangential velocity at peripheral wall of vortex tube after injected flow has been slowed down due to peripheral-wall friction, diffusion, and jet mixing, ft/sec

W_B Weight flow rate of simulated-buffer gas, lb/sec

$W_{B,TF}$ Weight flow rate of simulated-buffer gas removed through thru-flow ports, lb/sec

W_c Weight-flow rate of carrier gas in simulated-fuel mixture, lb/sec

W_F Weight-flow rate of simulated-fuel mixture, $W_c + W_I$, lb/sec

W_I Weight-flow rate of iodine in simulated fuel mixture, lb/sec

w_F Total amount of simulated fuel contained in vortex tube, lb

β_t Secondary flow similarity parameter, $(D/L)\left(Re_{t,p}^{0.8}\right)/Re_r$, dimensionless

ρ_B Density of simulated-buffer gas at injection, lb/ft^3

ρ_F Local simulated-fuel density at a given radius, lb/ft^3

$\bar{\rho}_F$ Average simulated-fuel density, lb/ft^3

μ_B Laminar viscosity of simulated-buffer gas, lb/ft-sec

TABLE I

SUMMARY OF VORTEX TUBE GEOMETRIES TESTED

Vortex Tube	Bypass Configuration	Location of Thru-Flow Removal	Simulated-Buffer-Gas Injection System		Simulated-Fuel Injection System		Figures on Which Results are Presented	
			Configuration	Total Area, A_j	Configuration	Total Area, A_{F_j}	Containment	Radial Distributions
Multiple-Fixed-Port (Fig. 4b)	Peripheral Bypass	Right End Wall	2856 ports (24 axial rows of 119 ports; dia = 0.062 in.)(Figs. 4b, 5c and 6b)	3.75 sq in.	End-wall injection without swirl through 10 tubes at left end wall (Figs. 7a and 8a)	0.079 sq in.	Fig. 9	Fig. 10
					End-wall injection with swirl through 10 wall jets at left end wall (Figs. 7b and 8b)	0.225 sq in.		
					Peripheral-wall injection at axial mid-plane through 12 tubes (Figs. 7c and 8c)	0.095 sq in.		
Directed-Wall-Jet (Fig. 4a)	Axial Bypass	Left, Right and Both End Walls	150 wall jets (5 axial rows of 30 jets spaced at 72-deg intervals around periphery; slot width = 0.5 in., slot height = 0.045 in.)(Figs. 4a, 5a and 6a)	3.38 sq in.	End-wall injection without swirl through 10 tubes at left end wall (Figs. 7a and 8a)	0.079 sq in.	Fig. 11	Fig. 12
		Both End Walls					Fig. 13	Fig. 14
	No Bypass		75 wall jets (5 axial rows of 15 jets spaced at 72-deg intervals around periphery; slot width = 0.5 in., slot height = 0.045 in.)(Figs. 4a, 5a and 6a)	1.69 sq in.			Fig. 15	Fig. 16
	No Bypass and Axial Bypass							Fig. 17
	Axial Bypass		75 wall jets and 150 wall jets (Figs. 4a, 5a and 6a)	1.69 and 3.38 sq in.			Fig. 18 Fig. 20 Fig. 22	
			150 wall jets (Figs. 4a, 5a and 6a)	3.38 sq in.				Fig. 19 Fig. 21 Fig. 23

FIG. 1

SCHEMATIC DIAGRAMS OF NUCLEAR LIGHT BULB ENGINE AND DESIRED FLOW PATTERN

a) UNIT CAVITY OF NUCLEAR LIGHT BULB ENGINE

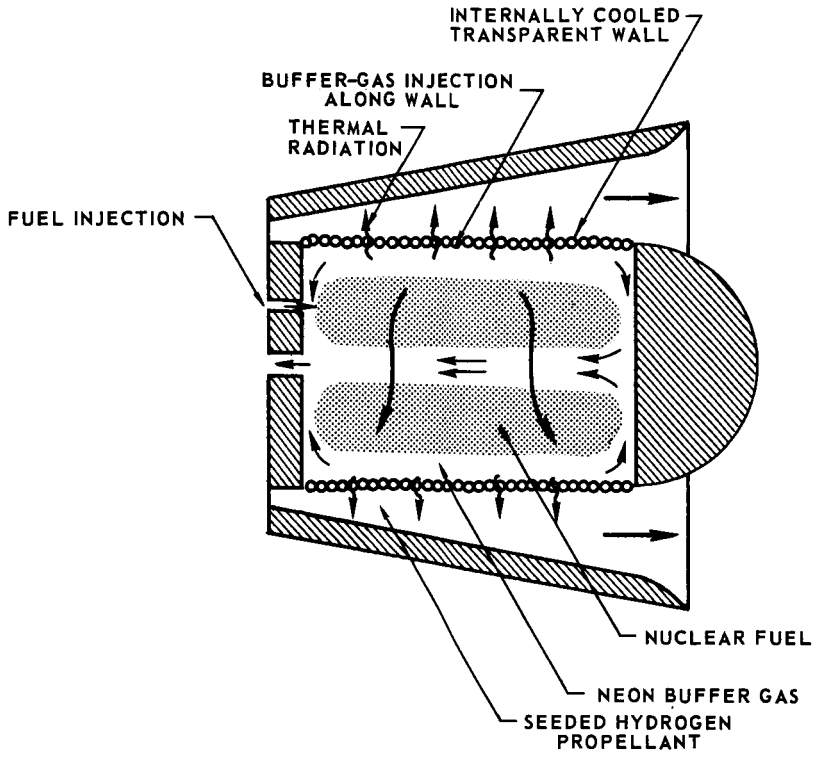

b) RADIAL-INFLOW FLOW PATTERN

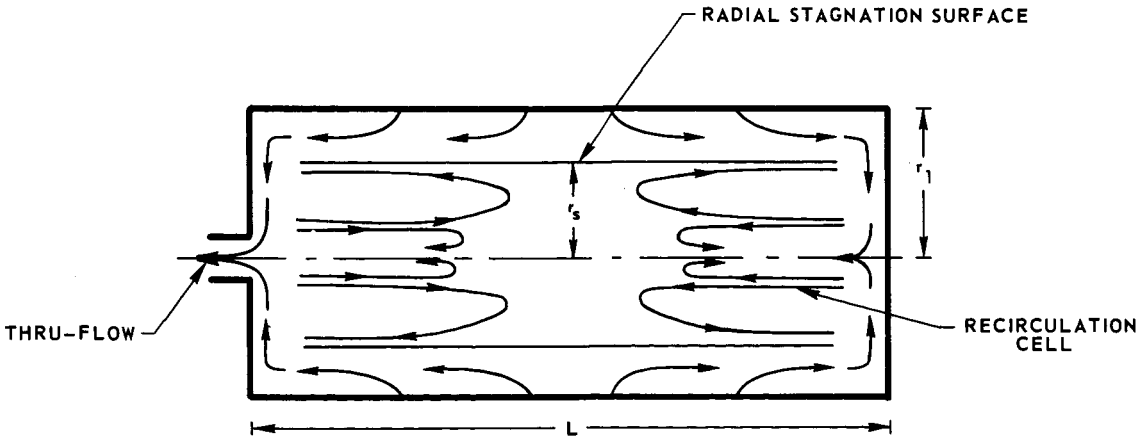

FIG. 2

SCHEMATIC DIAGRAM OF FLOW SYSTEM IN HIGH REYNOLDS NUMBER TEST FACILITY

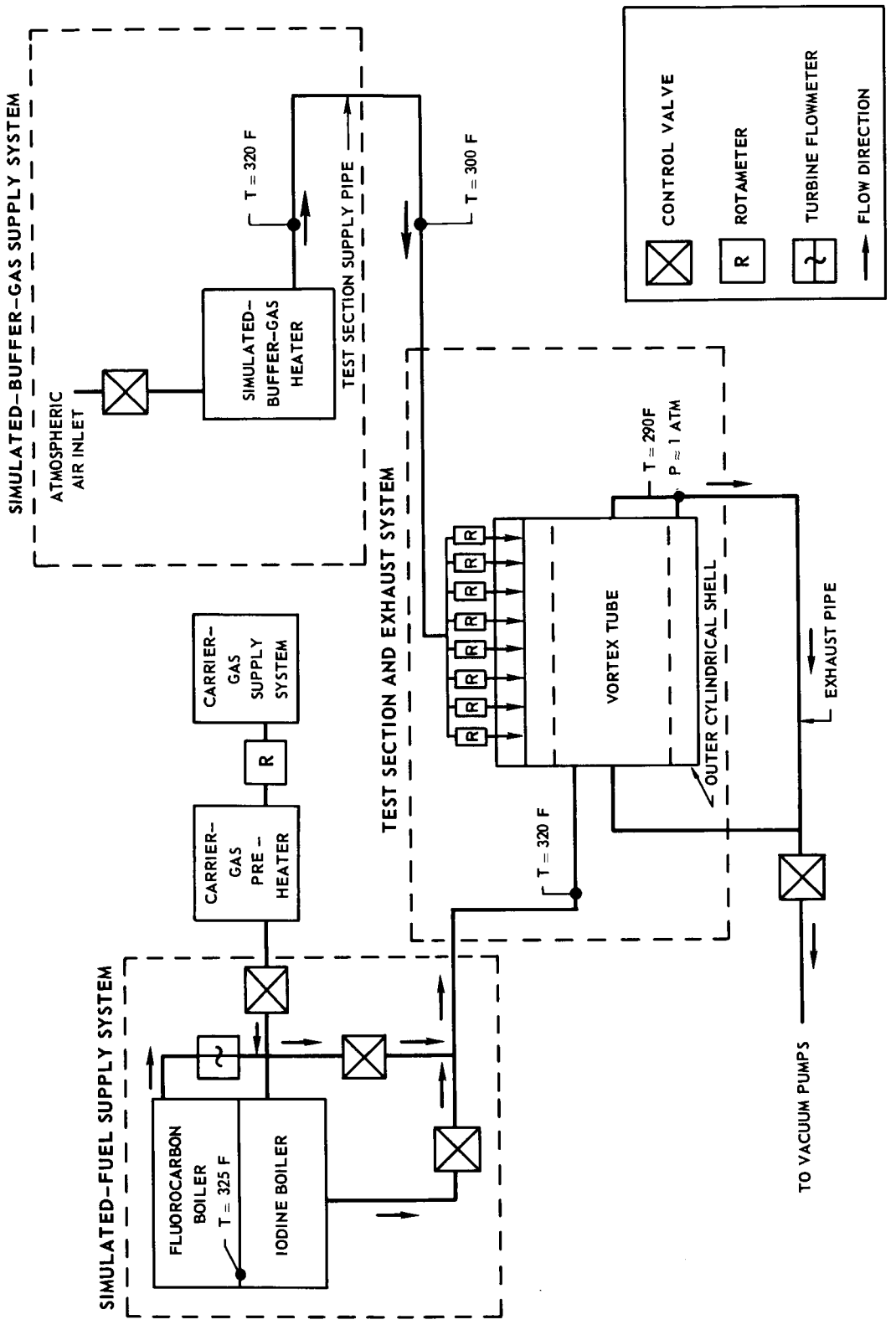

FIG. 3

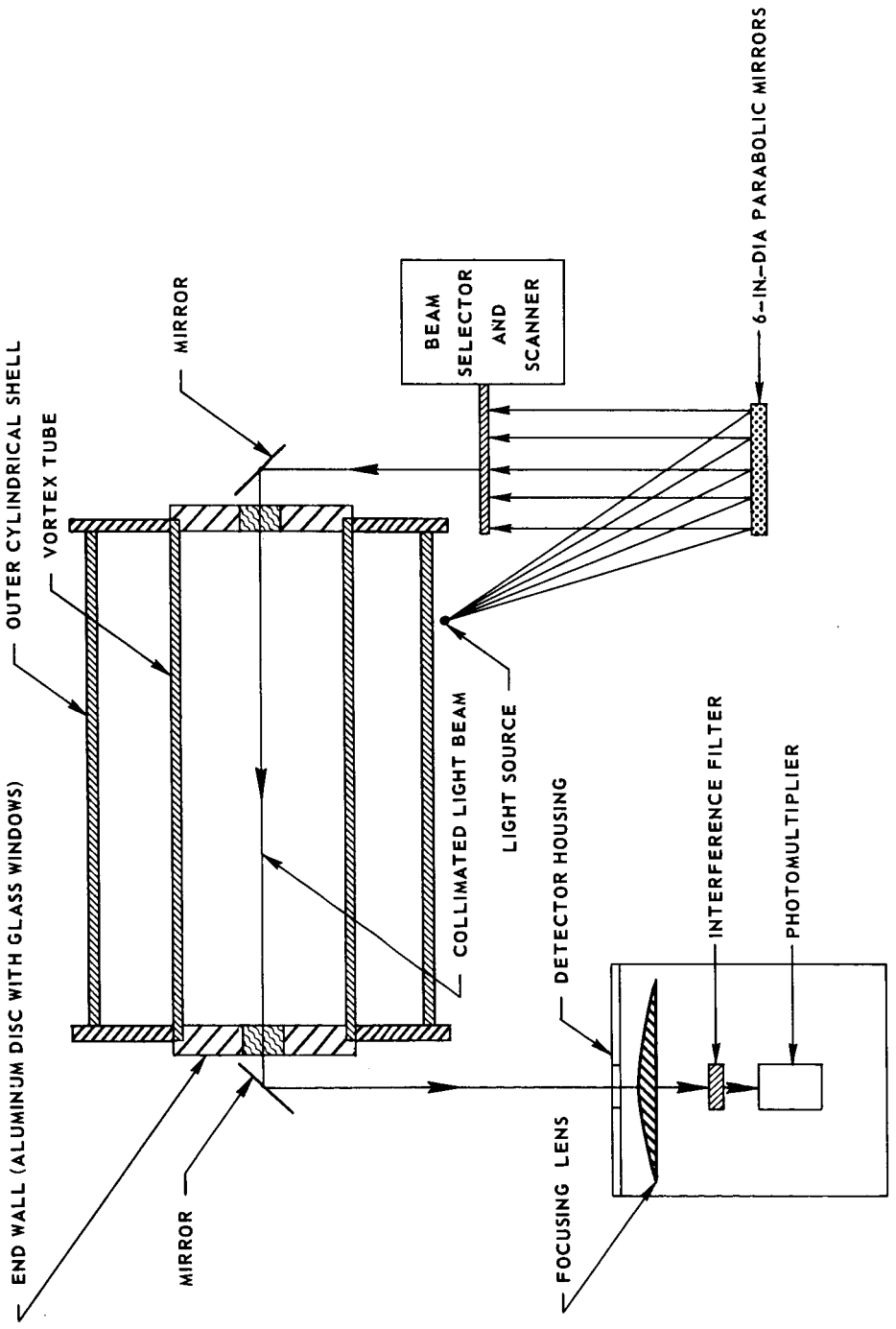
SCHEMATIC DIAGRAM OF AXIAL ABSORPTOMETER
DETAILS OF FLOW SYSTEM NOT SHOWN
LIGHT BEAM TRAVERSES PERPENDICULAR TO PLANE OF THIS VIEW
TOP VIEW
END WALL (ALUMINUM DISC WITH GLASS WINDOWS)
OUTER CYLINDRICAL SHELL
VORTEX TUBE
MIRROR
BEAM SELECTOR AND SCANNER
6-IN.-DIA PARABOLIC MIRRORS
COLLIMATED LIGHT BEAM
LIGHT SOURCE
DETECTOR HOUSING
INTERFERENCE FILTER
PHOTOMULTIPLIER
MIRROR
FOCUSING LENS

FIG. 4

PHOTOGRAPHS OF VORTEX TUBES

a) DIRECTED-WALL-JET VORTEX TUBE

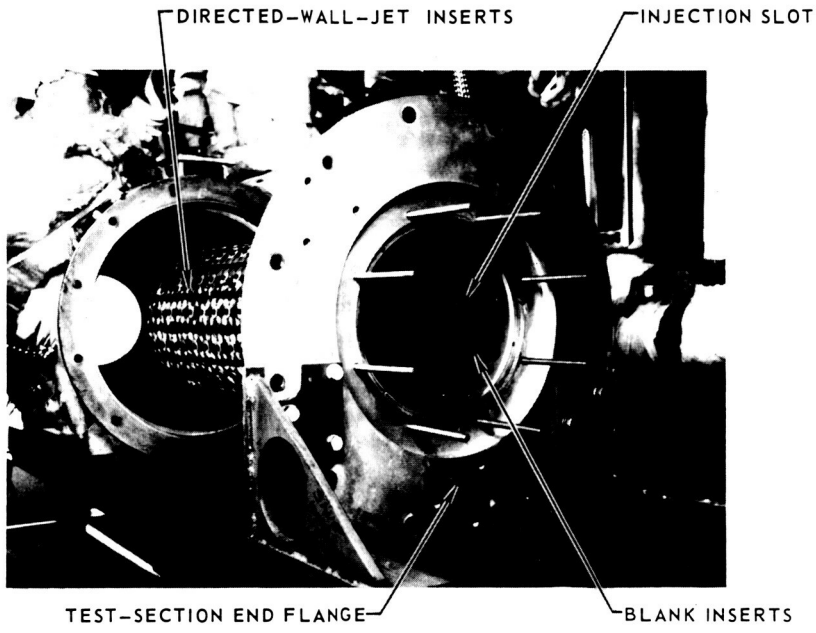

b) MULTIPLE-FIXED-PORT VORTEX TUBE

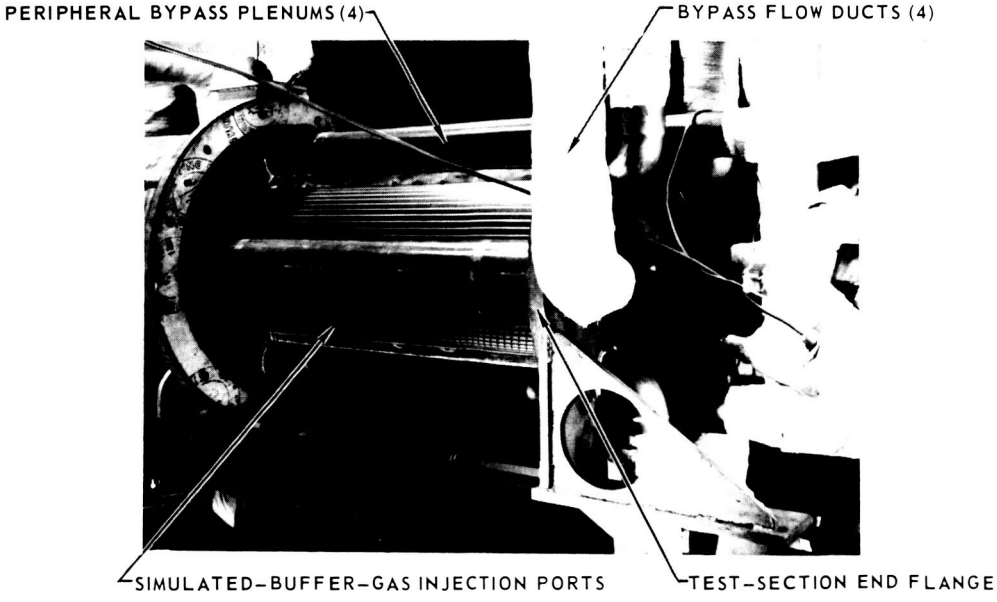

FIG. 5

DETAILS OF VORTEX TUBES

SEE FIG. 6 FOR DETAILS OF SIMULATED-BUFFER-GAS INJECTION CONFIGURATIONS AND FIGS. 7 AND 8 FOR DETAILS OF SIMULATED-FUEL INJECTION CONFIGURATIONS

ALL DIMENSIONS IN INCHES

a) DIRECTED-WALL-JET VORTEX TUBE WITH AXIAL BYPASS

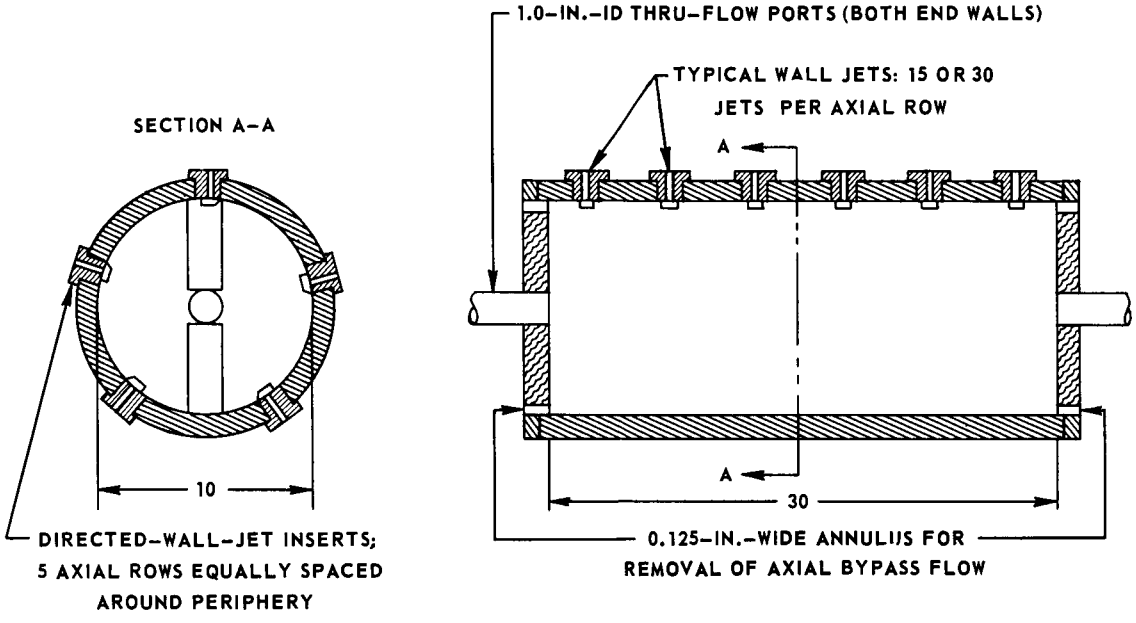

b) MULTIPLE-FIXED-PORT VORTEX TUBE WITH PERIPHERAL BYPASS

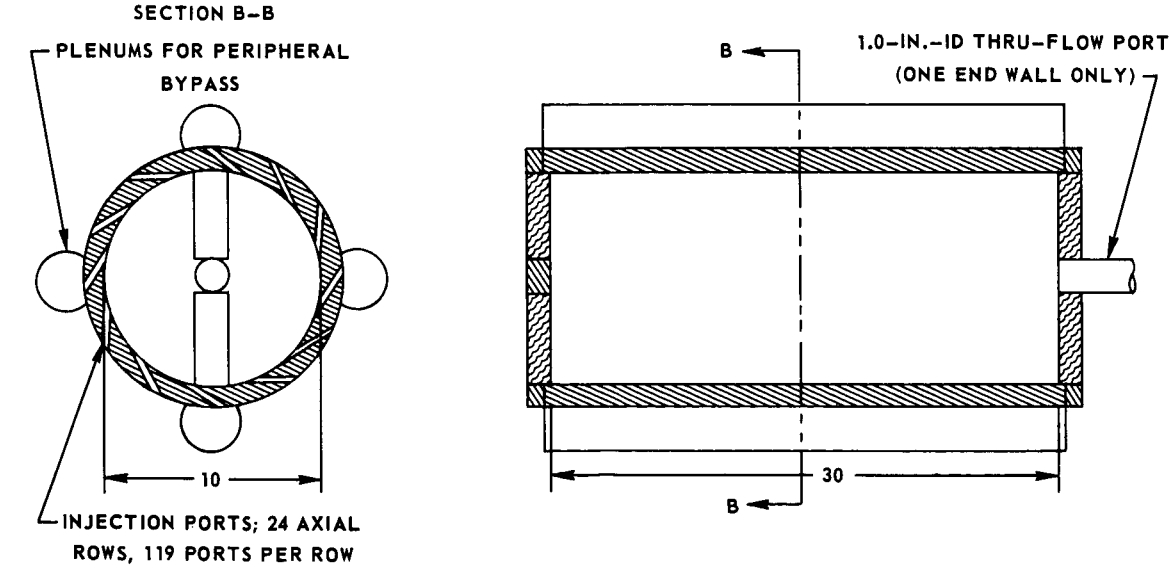

DETAILS OF SIMULATED-BUFFER-GAS INJECTION CONFIGURATIONS

SEE FIG. 5 FOR DETAILS OF VORTEX TUBES
ALL DIMENSIONS IN INCHES

a) DIRECTED-WALL-JET INJECTION

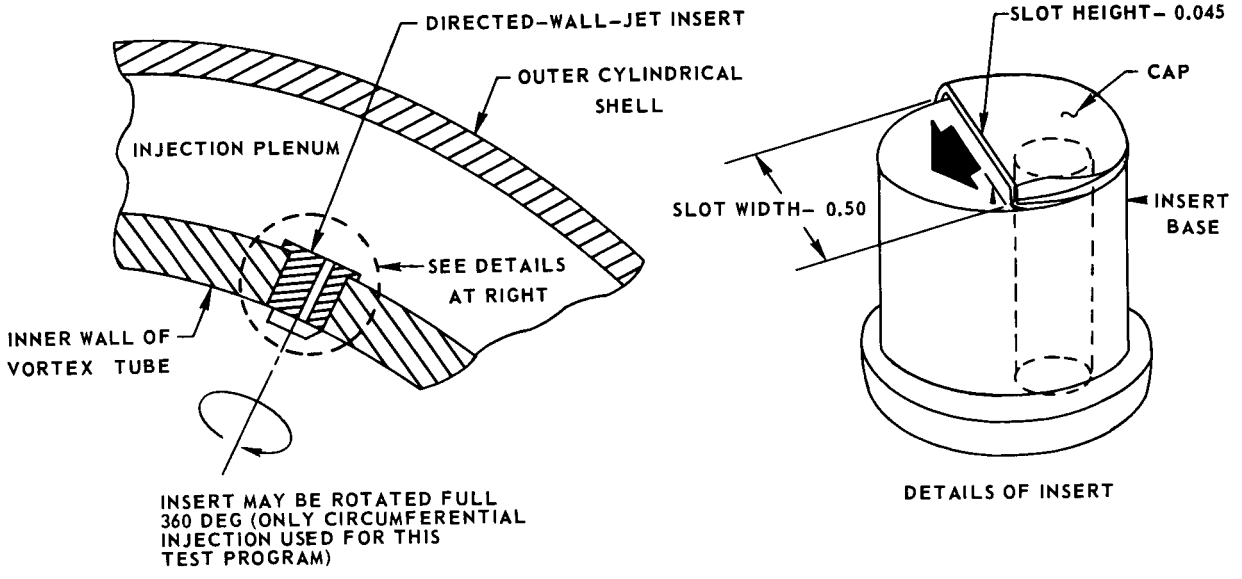

b) MULTIPLE-FIXED-PORT INJECTION

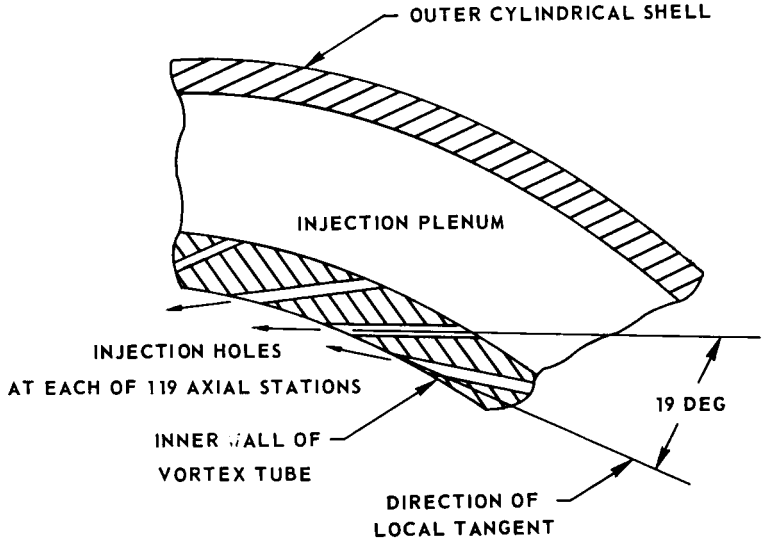

FIG. 7

DETAILS OF SIMULATED-FUEL INJECTION CONFIGURATIONS

SEE FIG. 5 FOR DETAILS OF VORTEX TUBES AND FIG. 8 FOR PHOTOGRAPHS

ALL DIMENSIONS IN INCHES

a) INJECTION FROM END WALL WITHOUT SWIRL

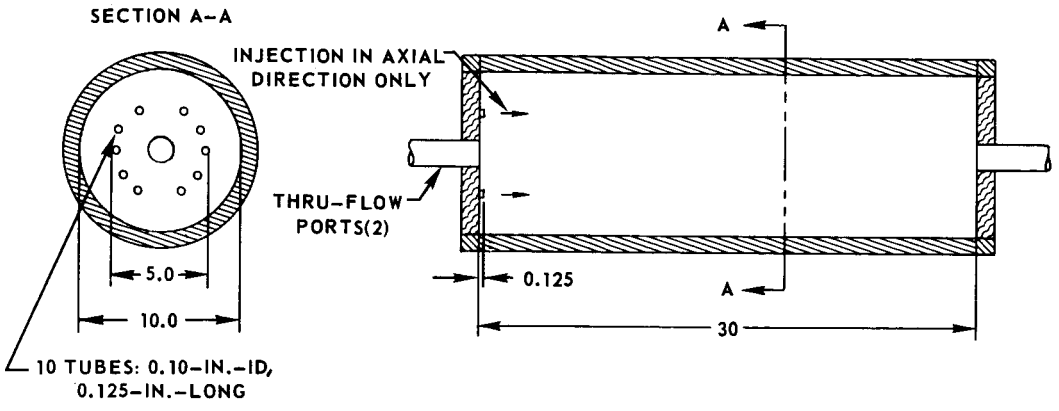

b) INJECTION FROM END WALL WITH SWIRL

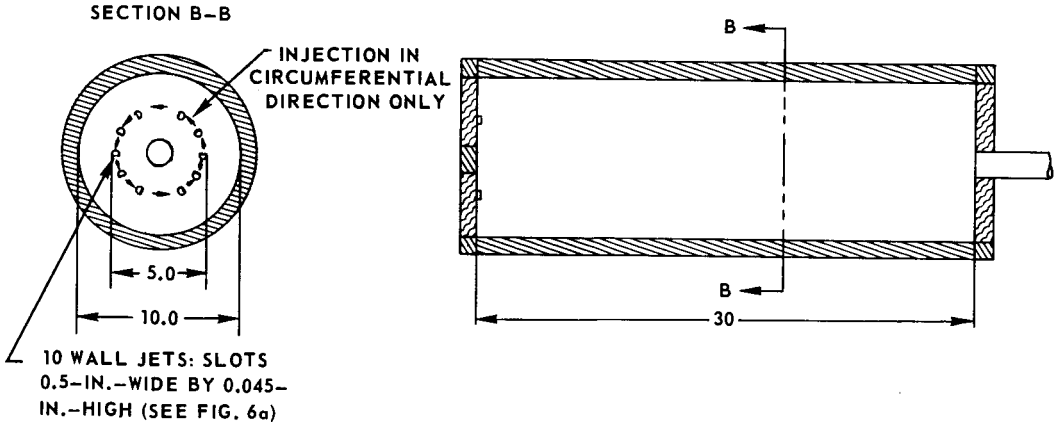

c) INJECTION FROM PERIPHERAL WALL

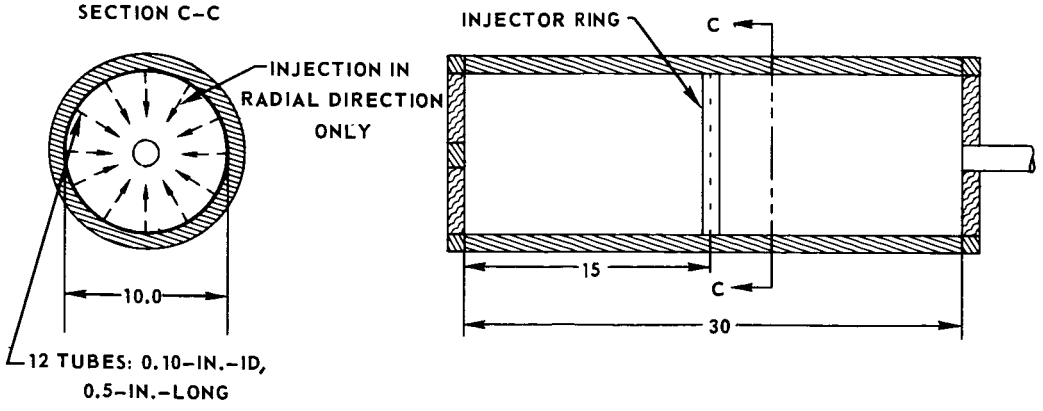

PHOTOGRAPHS OF SIMULATED-FUEL-INJECTION CONFIGURATIONS

SEE FIG. 7 FOR DETAILS

a) END WALL FOR INJECTION WITHOUT SWIRL

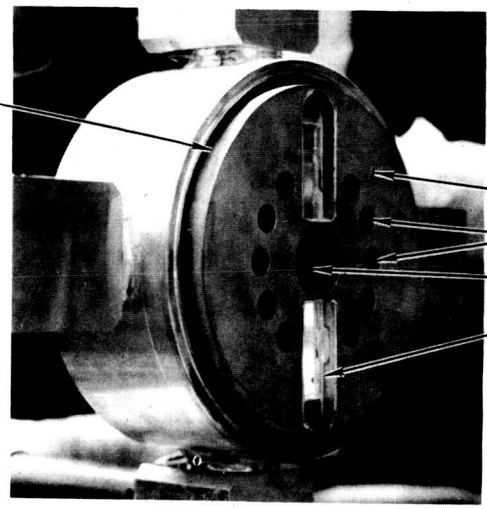

b) END WALL FOR INJECTION WITH SWIRL

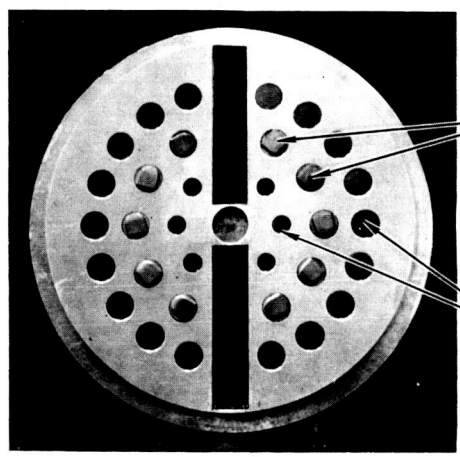

c) INJECTOR RING FOR PERIPHERAL-WALL INJECTION

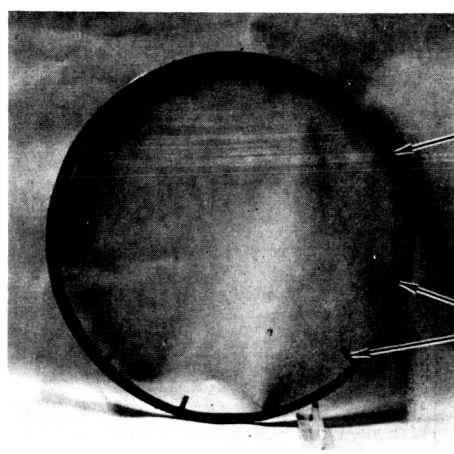

EFFECT OF CHANGES IN SIMULATED-FUEL INJECTION CONFIGURATION ON CONTAINMENT

MULTIPLE-FIXED-PORT VORTEX TUBE WITH PERIPHERAL BYPASS

SEE TABLE I AND FIGS. 4 THROUGH 8 FOR DETAILS OF CONFIGURATIONS TESTED

SIMULATED FUEL--FLUOROCARBON/IODINE MIXTURE, $m_F = 400$

SYMBOL	$Re_{t,j}$	W_B-LB/SEC	W_B/W_F	SIMULATED-FUEL INJECTION CONFIGURATION	β_t
○	263,000	0.60	19	END WALL WITHOUT SWIRL	$7000/Re_r$
△	264,000	0.60	58	END WALL WITHOUT SWIRL	↓
●	264,000	0.60	19	END WALL WITH SWIRL	↓
□	187,000	0.44	41	PERIPHERAL WALL AT AXIAL MID-PLANE	$5300/Re_r$

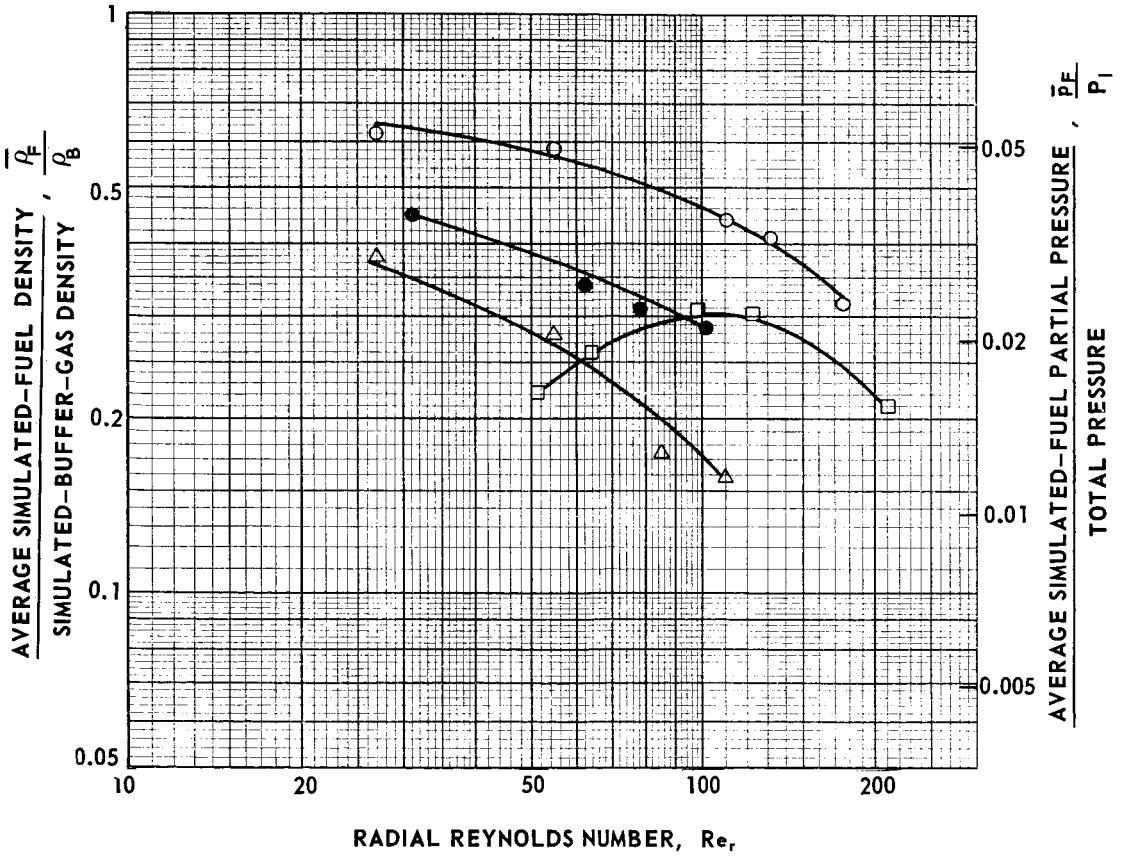

EFFECT OF CHANGES IN SIMULATED-FUEL INJECTION CONFIGURATION ON RADIAL DISTRIBUTION OF SIMULATED FUEL

SEE FIG. 9 FOR CORRESPONDING CONTAINMENT DATA

MULTIPLE-FIXED-PORT VORTEX TUBE WITH PERIPHERAL BYPASS

SEE TABLE I AND FIGS. 4 THROUGH 8 FOR DETAILS OF CONFIGURATIONS TESTED

SIMULATED FUEL--FLUOROCARBON/IODINE MIXTURE, $m_F = 400$

$Re_r \approx 100$ (CONSTANT)

SYMBOL	$Re_{t,j}$	W_B-LB/SEC	W_B/W_F	SIMULATED-FUEL INJECTION CONFIGURATION	β_t
○	263,000	0.60	19	END WALL WITHOUT SWIRL	70
△	264,000	0.60	58	END WALL WITHOUT SWIRL	70
●	264,000	0.60	19	END WALL WITH SWIRL	70
□	187,000	0.44	41	PERIPHERAL WALL AT AXIAL MID-PLANE	53

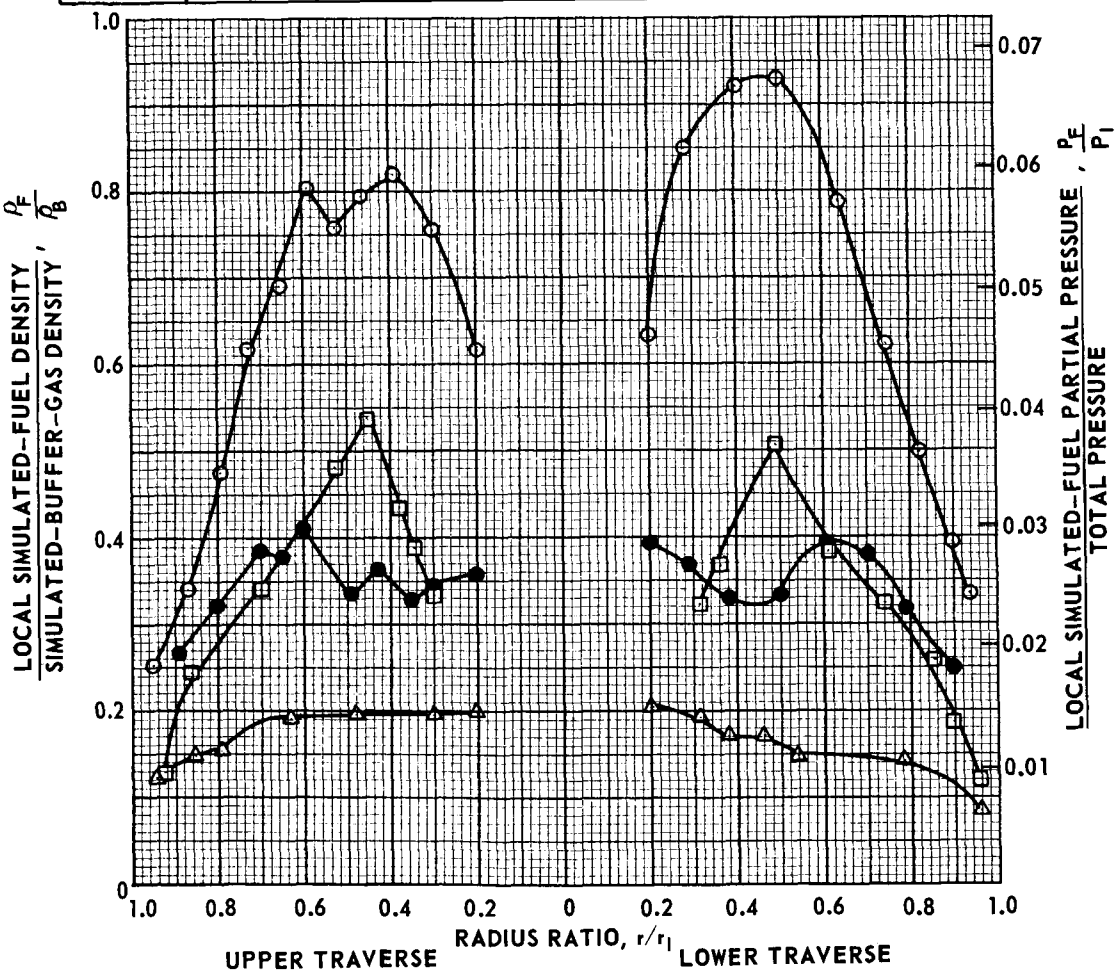

FIG. 11

EFFECT OF CHANGES IN THRU-FLOW CONFIGURATION ON CONTAINMENT

DIRECTED-WALL-JET VORTEX TUBE

SEE TABLE I AND FIGS. 4 THROUGH 8 FOR DETAILS OF CONFIGURATIONS TESTED

SIMULATED FUEL-- SULFUR-HEXAFLUORIDE/IODINE MIXTURE, $m_F = 146$

SIMULATED-BUFFER-GAS INJECTION AREA, $A_j = 3.38$ SQ IN.

$Re_r \approx 100$ (CONSTANT), PERCENT BYPASS = 90 (CONSTANT)

$W_B = 0.24$ (CONSTANT), $Re_{t,j} = 270{,}000$ (CONSTANT), $\beta_t = 58$

SYMBOL	THRU-FLOW PORTS USED
○	LEFT END WALL
△	RIGHT END WALL
□	BOTH END WALLS

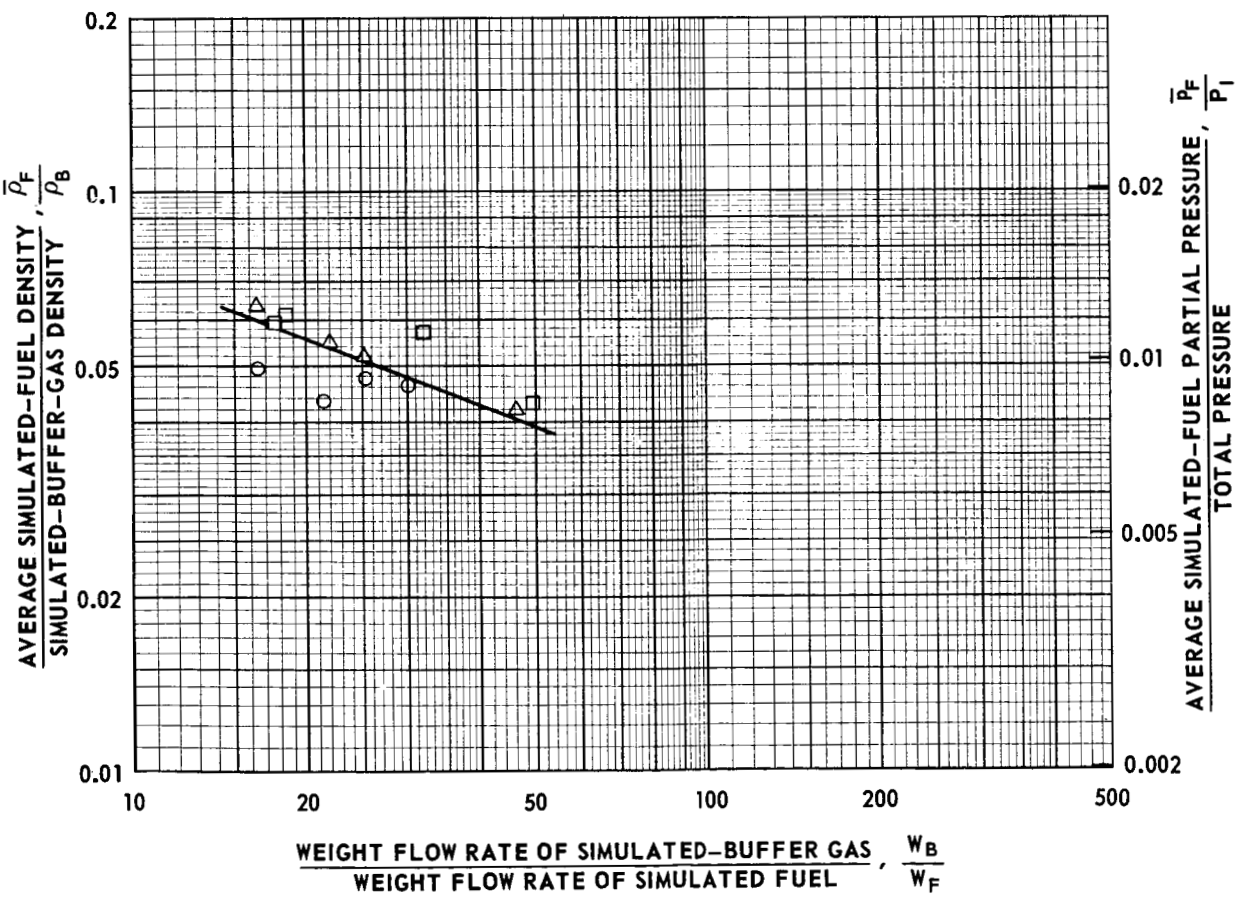

FIG. 12

EFFECT OF CHANGES IN THRU-FLOW CONFIGURATION ON RADIAL DISTRIBUTION OF SIMULATED FUEL

SEE FIG. 11 FOR CORRESPONDING CONTAINMENT DATA

DIRECTED-WALL-JET VORTEX TUBE

SEE TABLE I AND FIGS. 4 THROUGH 8 FOR DETAILS OF CONFIGURATIONS TESTED

SIMULATED FUEL--SULFUR-HEXAFLUORIDE/IODINE MIXTURE, $m_F = 146$

SIMULATED-BUFFER-GAS INJECTION AREA, $A_j = 3.38$ SQ IN.

$Re_r \approx 100$ (CONSTANT), PERCENT BYPASS = 90 (CONSTANT),
$W_B = 0.240$ (CONSTANT), $Re_{t,j} = 270{,}000$ (CONSTANT), $\beta_t = 58$

SYMBOL	W_B/W_F	THRU-FLOW PORTS USED
○	16.6	LEFT END WALL
△	16.6	RIGHT END WALL
□	17.2	BOTH END WALLS

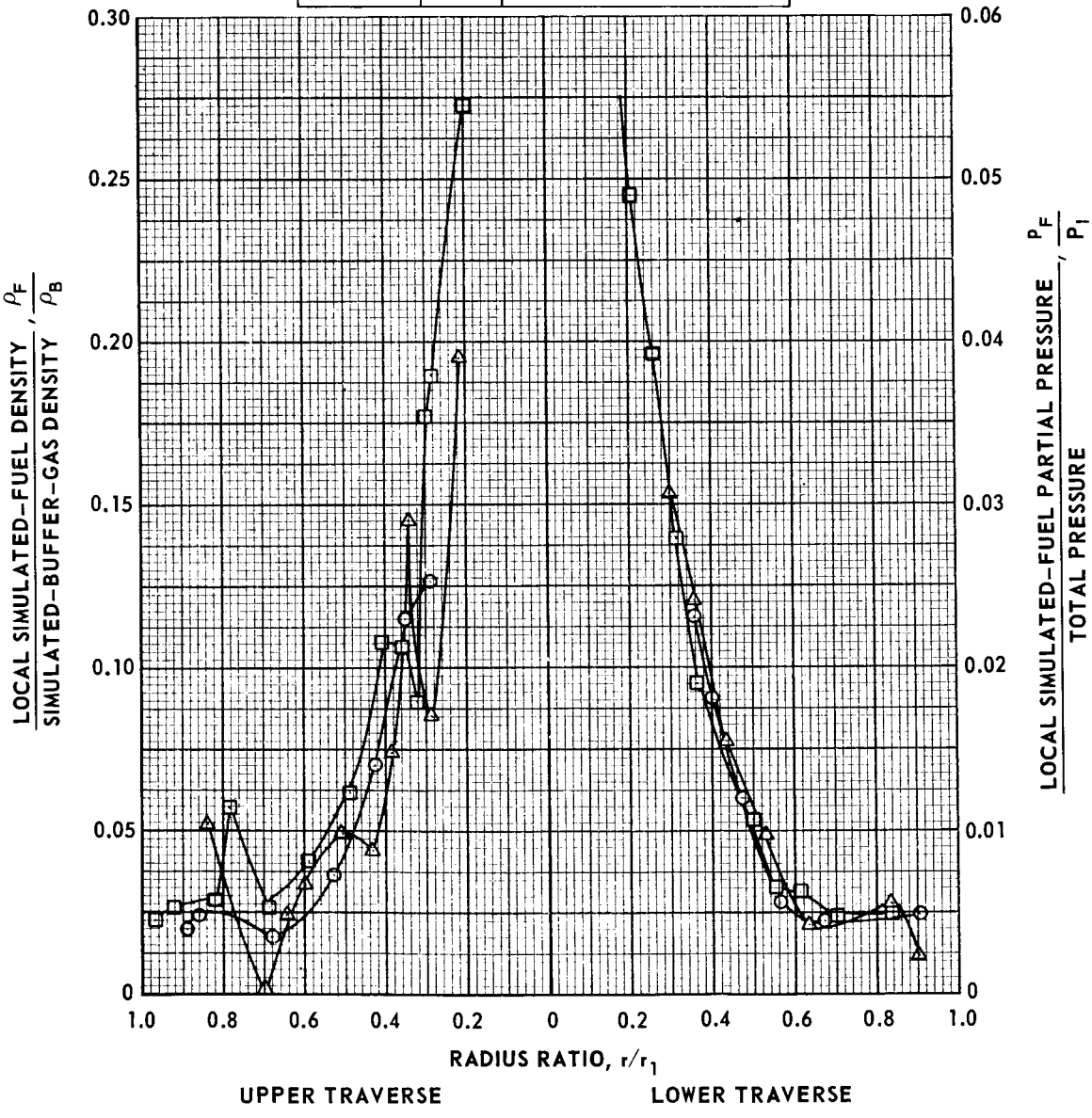

EFFECT OF RADIAL REYNOLDS NUMBER ON SIMULATED-FUEL CONTAINMENT

DIRECTED-WALL-JET VORTEX TUBE

SEE TABLE I AND FIGS. 4 THROUGH 8 FOR DETAILS OF CONFIGURATION

SIMULATED FUEL--SULFUR-HEXAFLUORIDE/IODINE MIXTURE; $m_F = 146$

SIMULATED-BUFFER-GAS INJECTION AREA, $A_j = 3.38$ SQ IN.

$W_B \approx 0.240$ LB/SEC (CONSTANT)

$Re_{t,j} \approx 270{,}000$ (CONSTANT)

SYMBOL	Re_r	PERCENT BYPASS	β_t
○	0	100	∞
△	54	95	109
□	106	90	55
◇	209	78	28

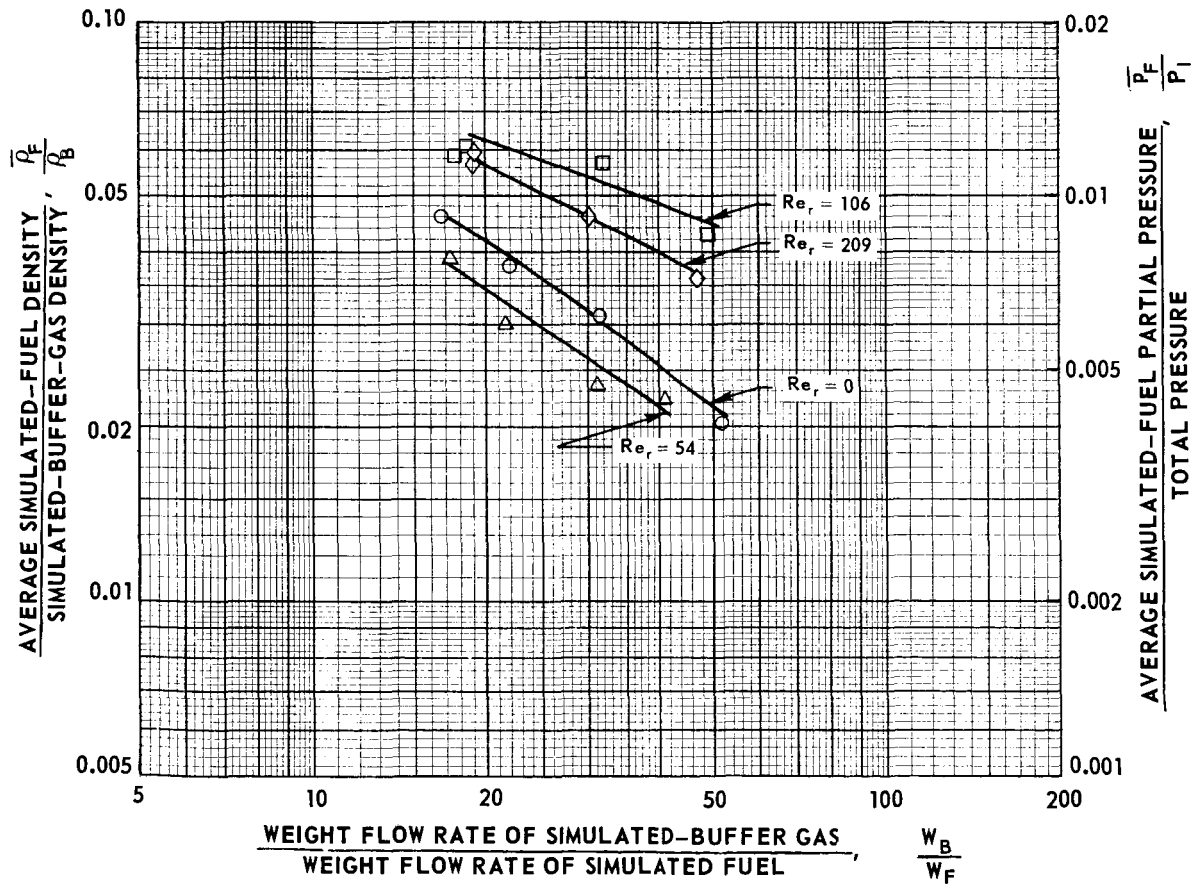

FIG. 14

EFFECT OF RADIAL REYNOLDS NUMBER ON RADIAL DISTRIBUTION OF SIMULATED FUEL

SEE FIG. 13 FOR CORRESPONDING CONTAINMENT DATA

DIRECTED-WALL-JET VORTEX TUBE

SEE TABLE I AND FIGS. 4 THROUGH 8 FOR DETAILS OF CONFIGURATION

SIMULATED FUEL-- SULFUR-HEXAFLUORIDE/IODINE MIXTURE; $m_F = 146$

SIMULATED-BUFFER-GAS INJECTION AREA, $A_j = 3.38$ SQ IN.

$W_B \approx 0.240$ LB/SEC (CONSTANT), $Re_{r,j} = 270{,}000$ (CONSTANT)

SYMBOL	Re_r	W_B/W_F	PERCENT BYPASS	β_t
○	0	31.3	100	∞
△	54	31.2	95	109
□	106	32.1	90	55
◇	209	31.6	78	28

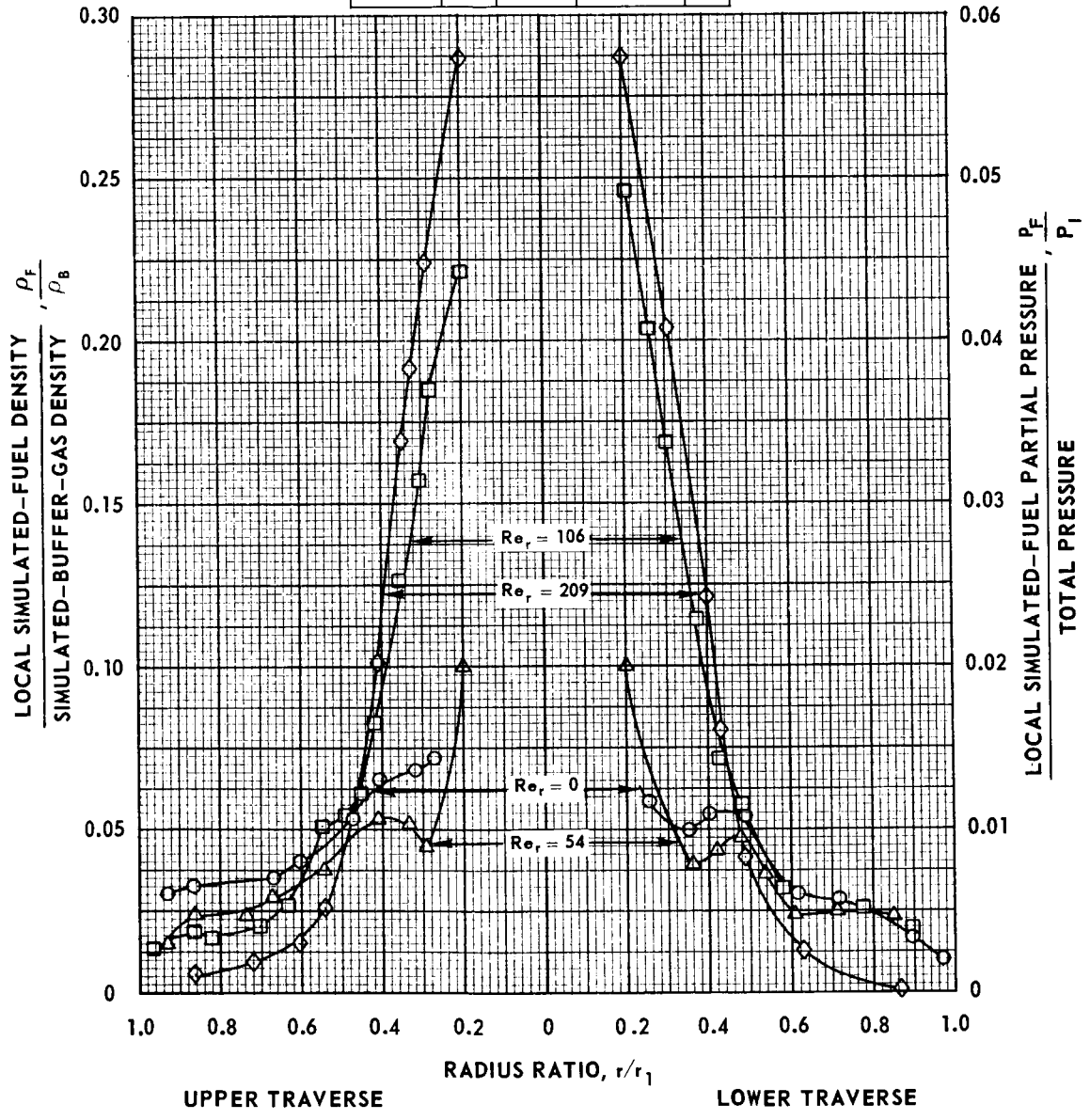

FIG. 15

SIMULATED-FUEL CONTAINMENT WITH NO BYPASS FLOW WITHDRAWAL

DIRECTED-WALL-JET VORTEX TUBE

SEE TABLE I AND FIGS. 4 THROUGH 8 FOR DETAILS OF CONFIGURATION

SIMULATED FUEL--NITROGEN/IODINE MIXTURE; $m_F = 29$

SIMULATED-BUFFER-GAS INJECTION AREA, $A_j = 1.69$ SQ IN.

PERCENT BYPASS = 0 (CONSTANT)

SYMBOL	$Re_{t,j}$	Re_r	W_B-LB/SEC	β_t
○	30,600	56	0.0132	14.9
△	59,100	110	0.0257	12.8
□	114,000	214	0.0502	11.2

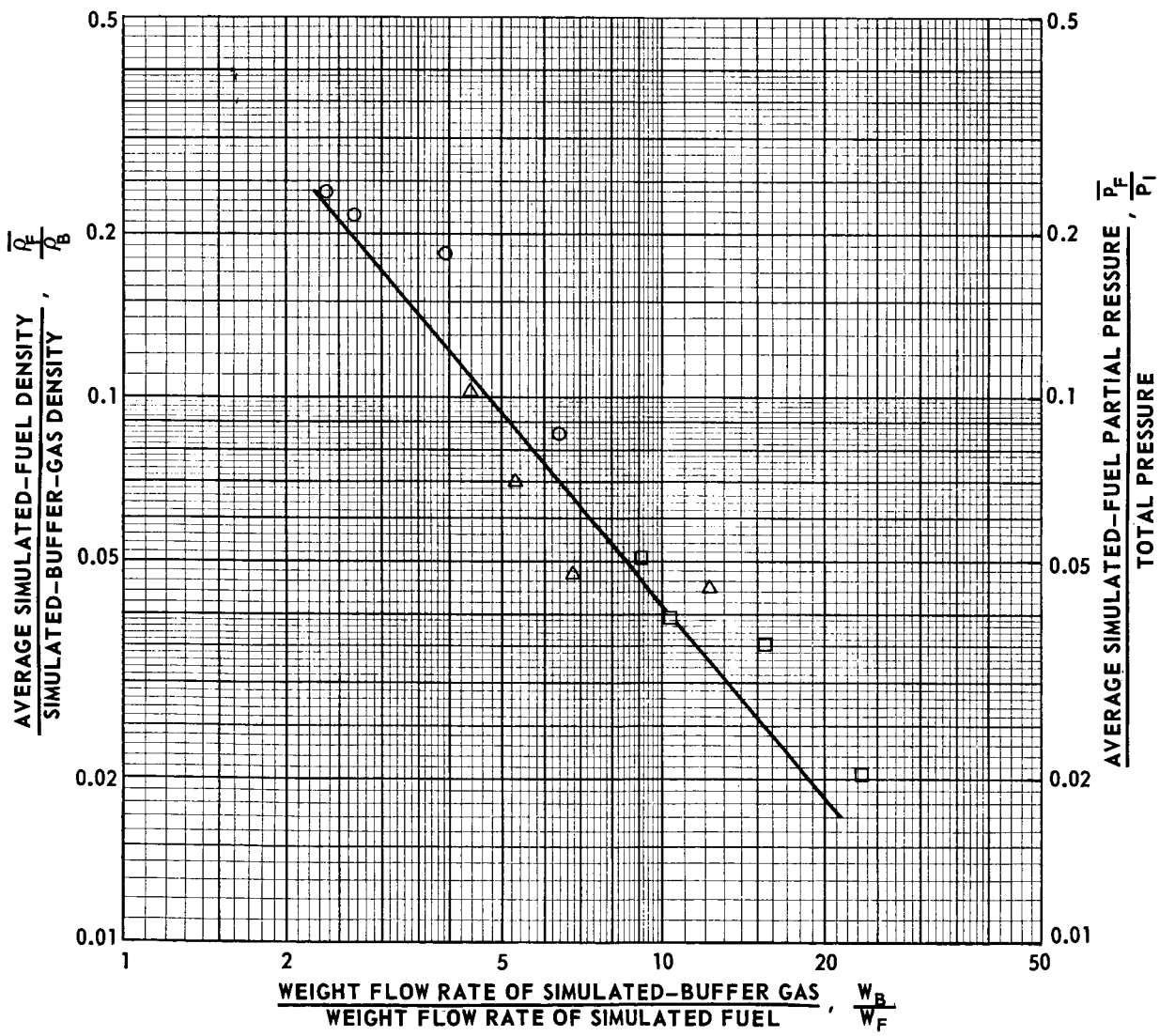

TYPICAL RADIAL DISTRIBUTIONS OF SIMULATED FUEL WITH NO BYPASS FLOW WITHDRAWAL

SEE FIG. 15 FOR CORRESPONDING CONTAINMENT DATA

DIRECTED-WALL-JET VORTEX TUBE

SEE TABLE I AND FIGS. 4 THROUGH 8 FOR DETAILS OF CONFIGURATION

SIMULATED FUEL--NITROGEN/IODINE MIXTURE; $m_F = 29$

SIMULATED-BUFFER-GAS INJECTION AREA, $A_j = 1.69$ SQ IN.

PERCENT BYPASS = 0 (CONSTANT)

$W_F = 0.0021$ LB/SEC (CONSTANT)

SYMBOL	$Re_{t,j}$	Re_r	W_B-LB/SEC	W_B/W_F	β_t
○	30,600	56	0.0132	6.4	14.9
△	59,100	110	0.0257	12.2	12.8
□	114,000	214	0.0502	23.5	11.2

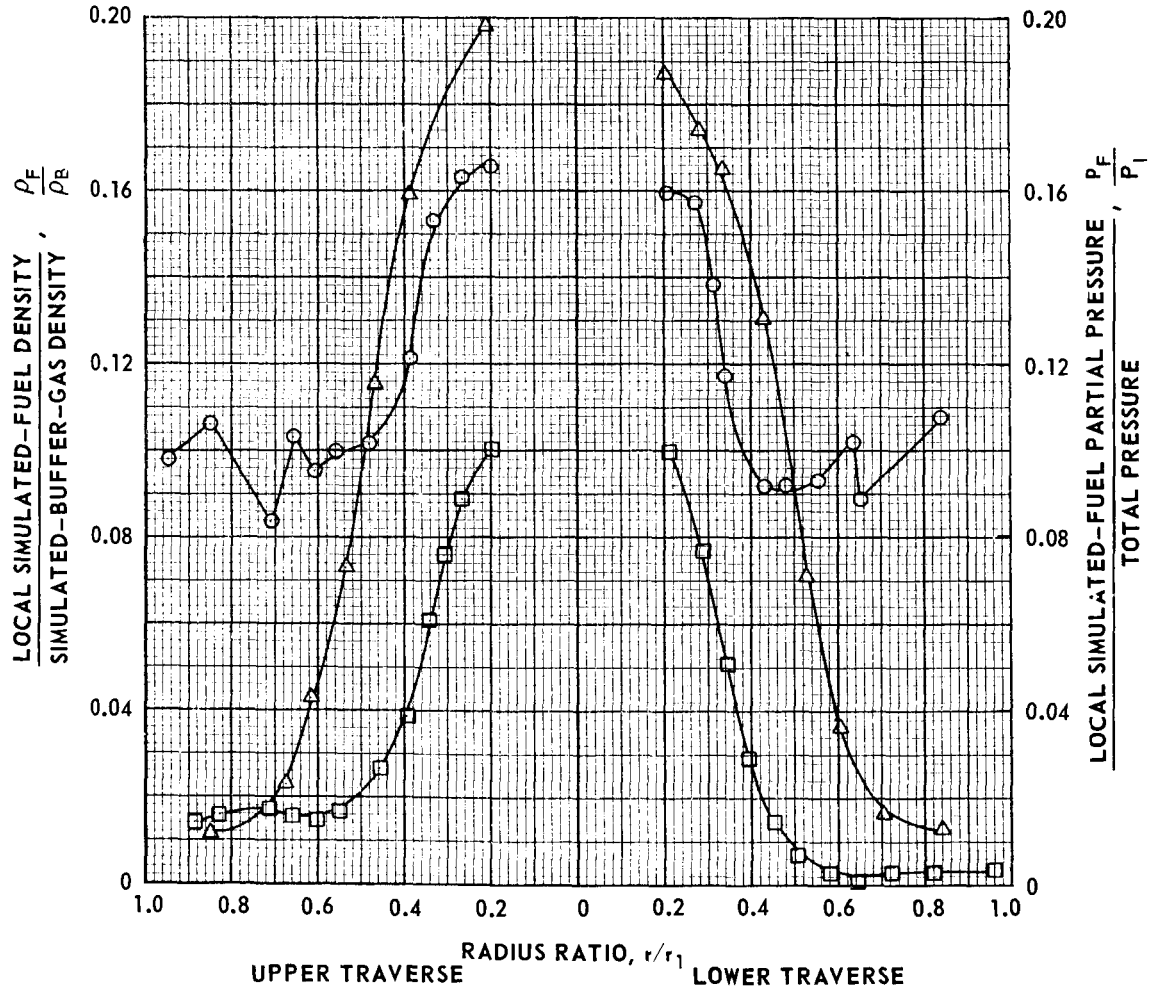

COMPARISON OF RADIAL DISTRIBUTIONS OF SIMULATED FUEL FOR VORTEXES WITH DIFFERENT TANGENTIAL REYNOLDS NUMBERS AND CONSTANT RADIAL REYNOLDS NUMBER

DIRECTED-WALL-JET VORTEX TUBE

SEE TABLE I AND FIGS.4 THROUGH 8 FOR DETAILS OF CONFIGURATION

SIMULATED FUEL--NITROGEN/IODINE MIXTURE; $m_F = 29$

SIMULATED-BUFFER-GAS INJECTION AREA, $A_j = 1.69$ SQ IN.

$Re_r = 110$ (CONSTANT), $W_F = 0.0048$ LB/SEC (CONSTANT)

SYMBOL	$Re_{t,j}$	W_B-LB/SEC	$W_{B,TF}/W_F$	PERCENT BYPASS	β_t
○	59,100	.025	5.2	0	12.8
△	268,000	.120	5.2	79	43.1

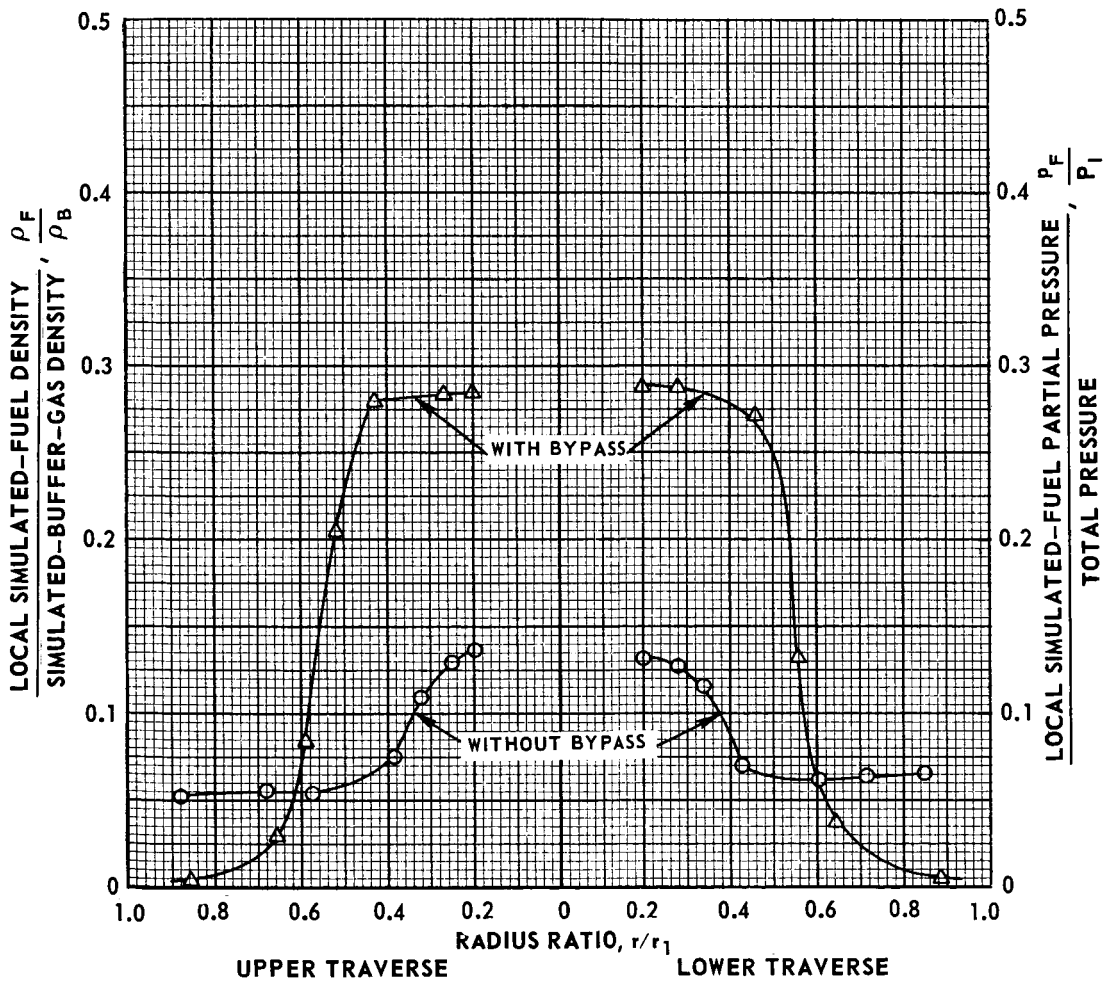

CONTAINMENT DATA OBTAINED WITH HELIUM/IODINE MIXTURE AS SIMULATED FUEL

DIRECTED-WALL-JET VORTEX TUBE

SEE TABLE I AND FIGS. 4 THROUGH 8 FOR DETAILS OF CONFIGURATION

$Re_r \approx 110$ (CONSTANT), $m_F = 5$

SYMBOL	A_j – SQ IN.	$Re_{t,j}$	W_B – LB/SEC	PERCENT BYPASS	β_t
○	1.69	268,000	0.12	79	43
△	3.38	136,000	0.12	79	31
□	3.38	272,000	0.24	90	54

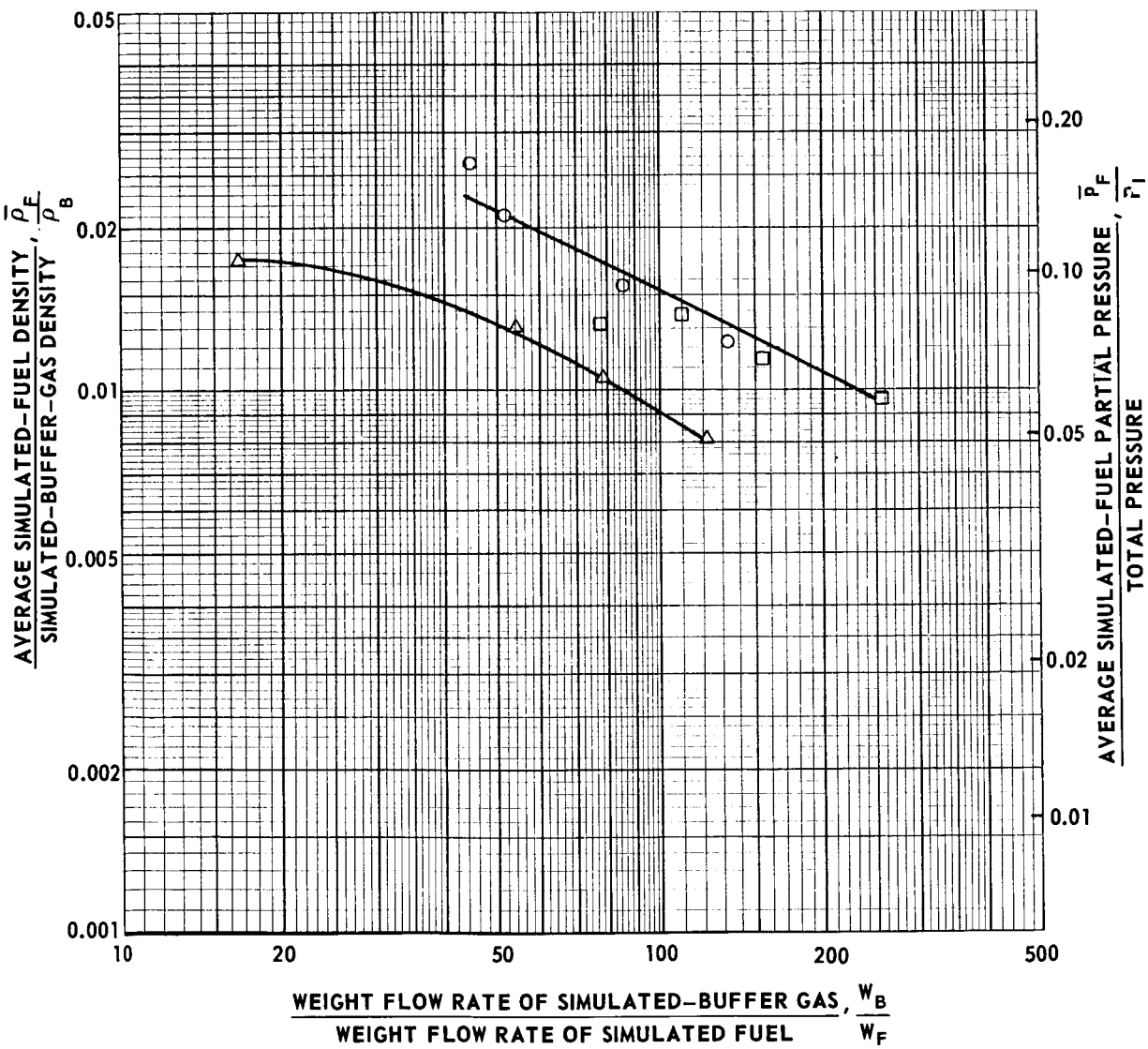

FIG. 19

RADIAL DISTRIBUTIONS OF SIMULATED FUEL OBTAINED WITH HELIUM/IODINE MIXTURE AS SIMULATED FUEL

SEE FIG. 18 FOR CORRESPONDING CONTAINMENT DATA

DIRECTED-WALL-JET VORTEX TUBE

SEE TABLE I AND FIGS. 4 THROUGH 8 FOR DETAILS OF CONFIGURATION

SIMULATED-BUFFER-GAS INJECTION AREA, $A_j = 3.38$ SQ IN.

CONSTANTS: $Re_r = 105$, PERCENT BYPASS = 90%,
$W_B = 0.240$ LB/SEC, $Re_{t,j} = 272{,}000$, $\beta_t = 54$, $m_F = 5$

SYMBOL	W_B/W_F
○	77
△	110
□	152
◇	251

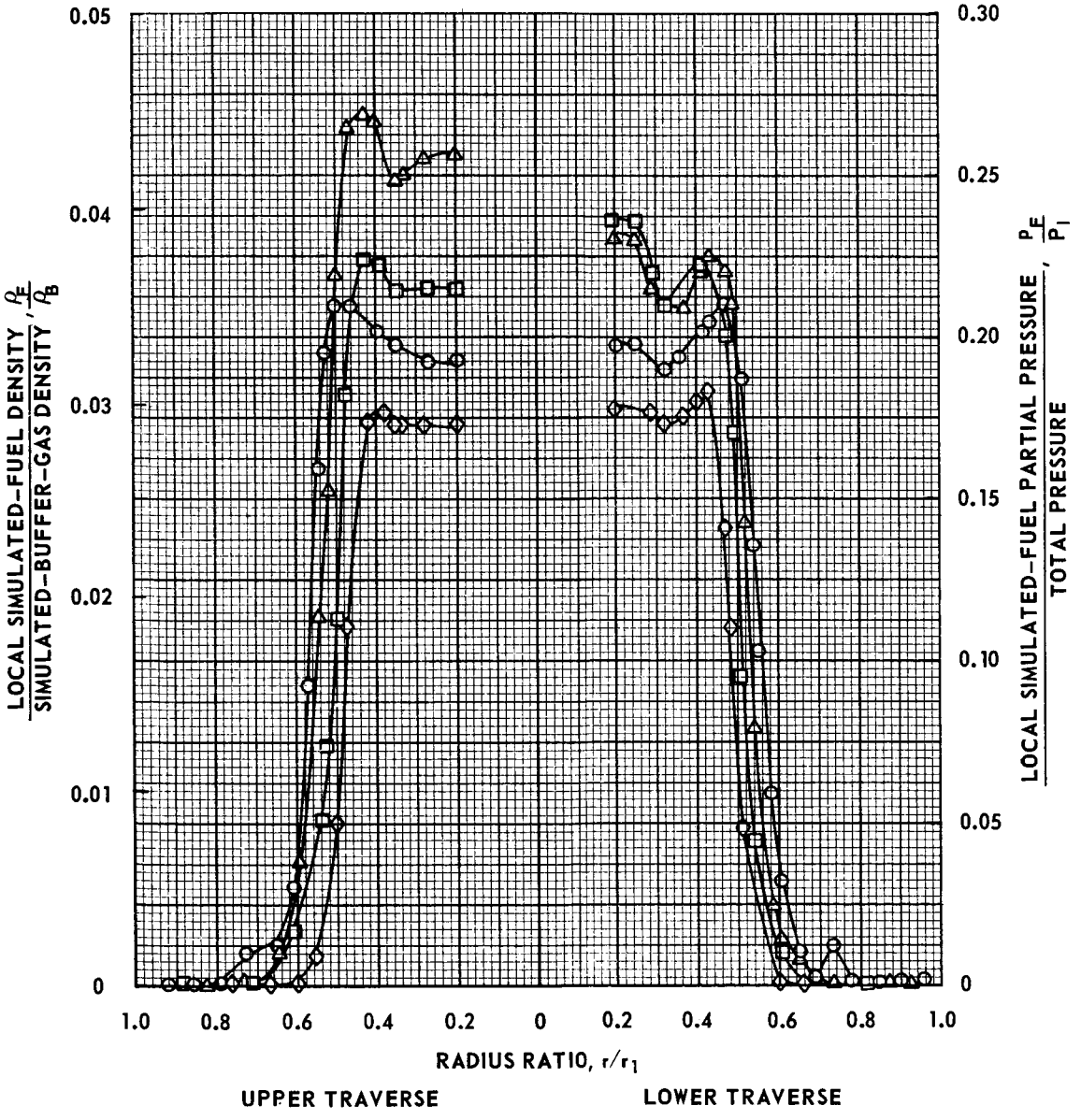

CONTAINMENT DATA OBTAINED WITH NITROGEN/IODINE MIXTURE AS SIMULATED FUEL

DIRECTED-WALL-JET VORTEX TUBE

SEE TABLE I AND FIGS. 4 THROUGH 8 FOR DETAILS OF CONFIGURATION

$Re_r \approx 110$ (CONSTANT), $m_F = 29$

SYMBOL	A_j –SQ IN.	$Re_{t,j}$	W_B–LB/SEC	PERCENT BYPASS	β_t
○	1.69	268,000	0.12	79	43
△	3.38	139,000	0.12	79	31
□	3.38	272,000	0.24	90	54

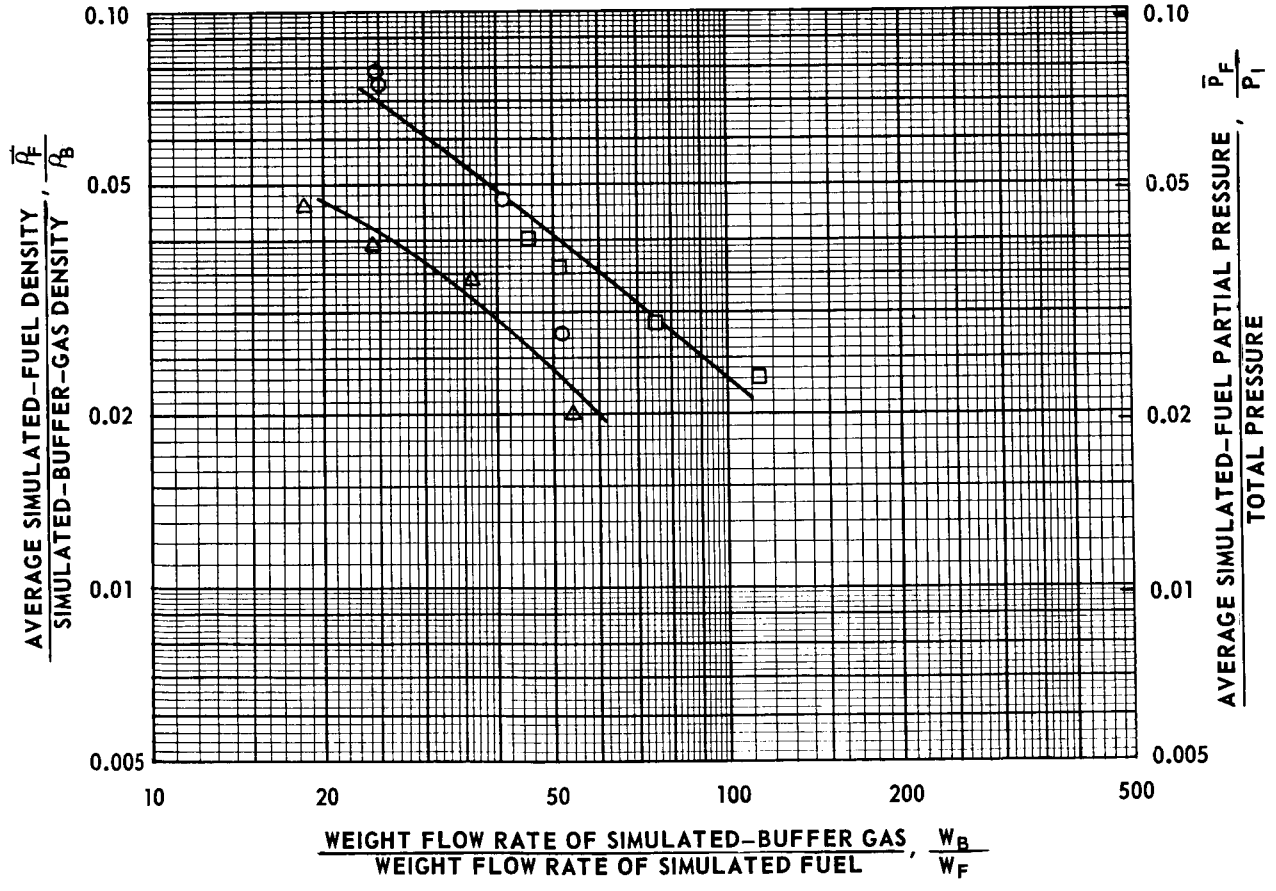

RADIAL DISTRIBUTIONS OF SIMULATED FUEL OBTAINED WITH NITROGEN/IODINE MIXTURE AS SIMULATED FUEL

SEE FIG. 20 FOR CORRESPONDING CONTAINMENT DATA

DIRECTED-WALL-JET VORTEX TUBE

SEE TABLE I AND FIGS. 4 THROUGH 8 FOR DETAILS OF CONFIGURATION

SIMULATED-BUFFER-GAS INJECTION AREA, A_j = 3.38 SQ IN.

CONSTANTS: Re_r = 107 , PERCENT BYPASS = 90%,

W_B = 0.240 LB/SEC , $Re_{t,j}$ = 272,000 , β_t = 54, m_F = 29

SYMBOL	W_B/W_F
○	45
△	50
□	77
◇	113

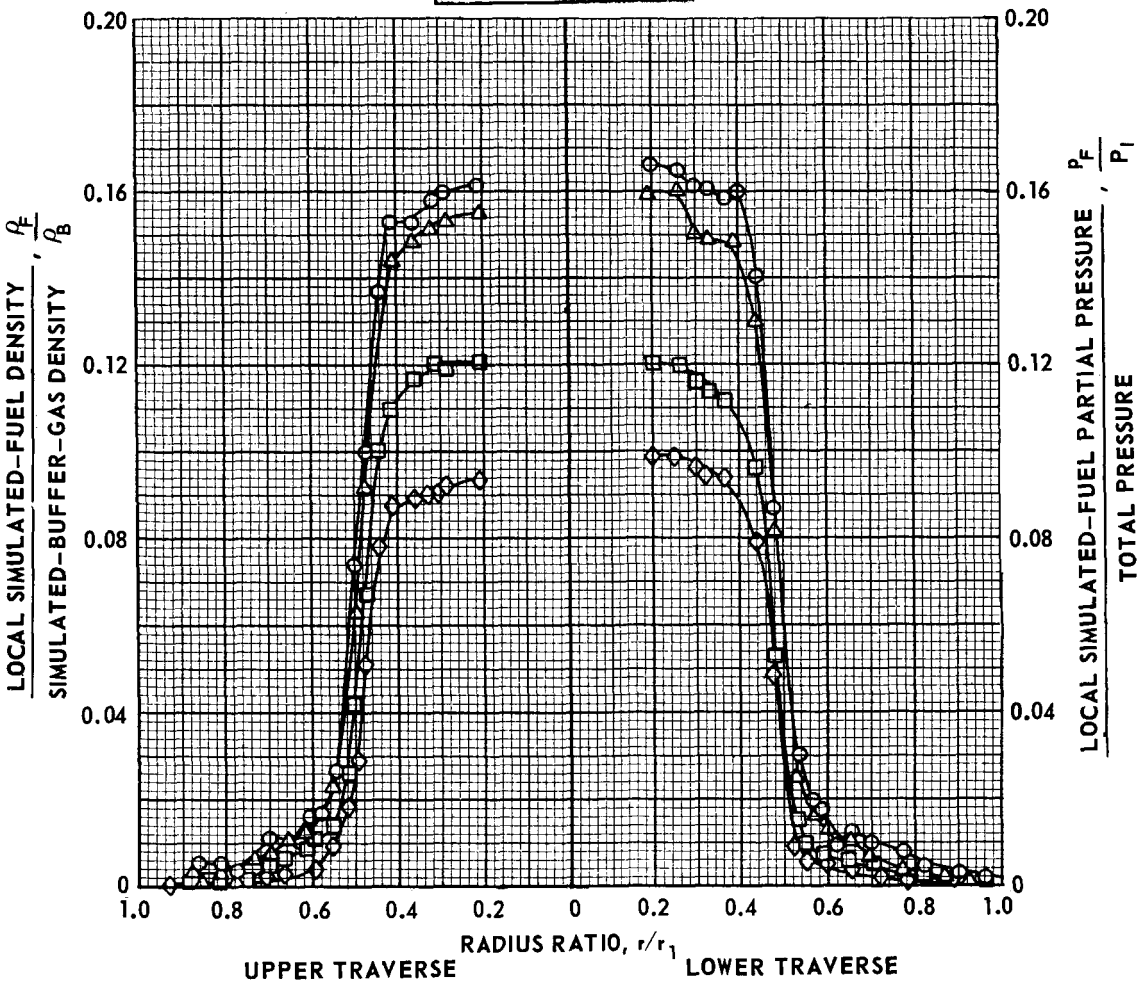

FIG. 22

CONTAINMENT DATA OBTAINED WITH SULFUR-HEXAFLUORIDE/IODINE MIXTURE AS SIMULATED FUEL

DIRECTED-WALL-JET VORTEX TUBE

SEE TABLE I AND FIGS. 4 THROUGH 8 FOR DETAILS OF CONFIGURATION

$Re_r \approx 110$ (CONSTANT), $m_F \approx 146$

SYMBOL	A_j -SQ IN.	$Re_{t,j}$	W_B -LB/SEC	PERCENT BYPASS	β_t
○	1.69	268,000	0.12	79	43
△	3.38	136,000	0.12	79	31
□	3.38	272,000	0.24	90	54

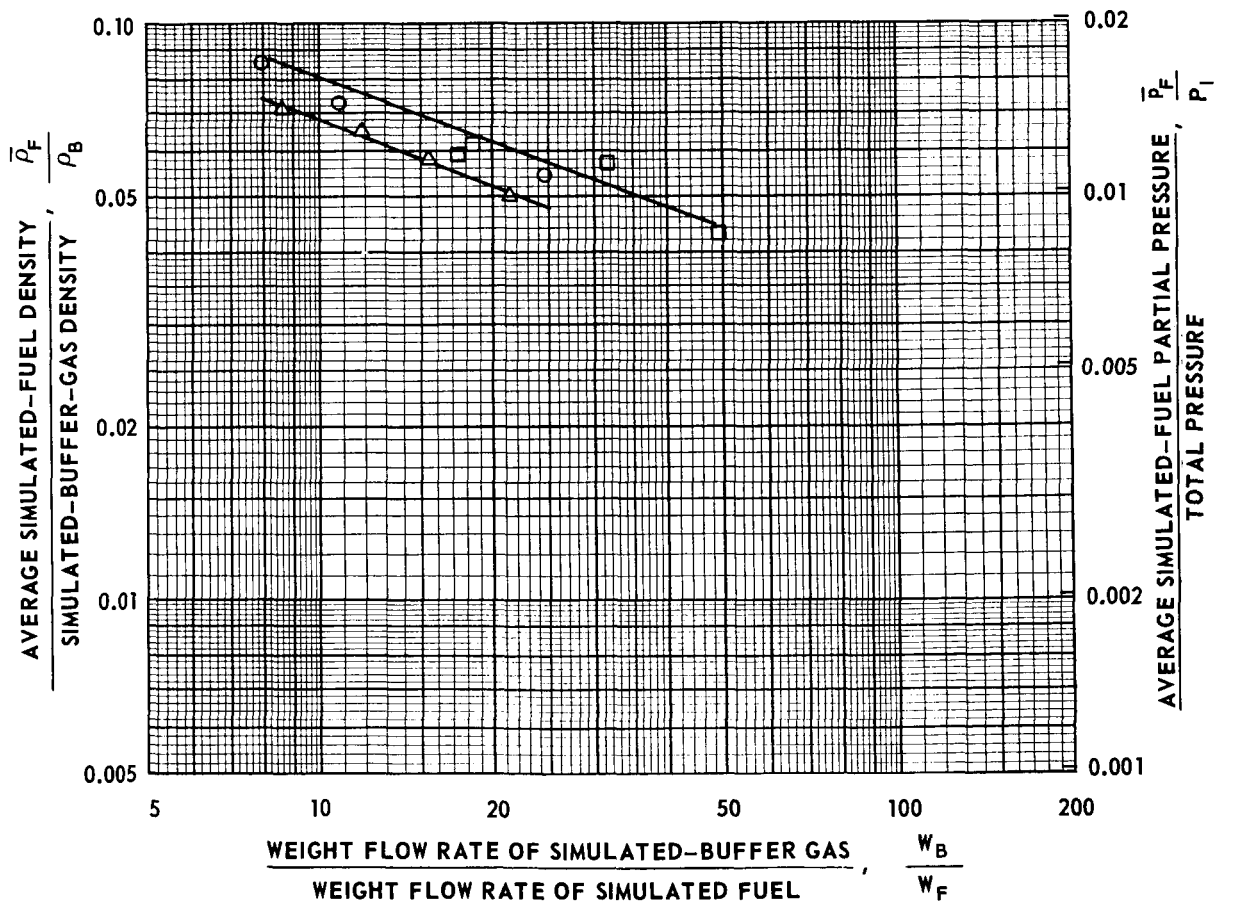

FIG. 23

RADIAL DISTRIBUTIONS OF SIMULATED FUEL OBTAINED WITH SULFUR-HEXAFLUORIDE/IODINE MIXTURE AS SIMULATED FUEL

SEE FIG. 22 FOR CORRESPONDING CONTAINMENT DATA

DIRECTED-WALL-JET VORTEX TUBE

SEE TABLE I AND FIGS. 4 THROUGH 8 FOR DETAILS OF CONFIGURATION

SIMULATED-BUFFER-GAS INJECTION AREA, A_j = 3.38 SQ IN.

CONSTANTS: Re_t = 106, PERCENT BYPASS = 90%.
W_B = 0.240 LB/SEC, $Re_{t,j}$ = 272,000, β_t = 54, m_F = 146

SYMBOL	W_B/W_F
○	17.2
△	18.2
□	32.1
◇	49.2